

Models and Information Rates for Wiener Phase Noise Channels

Hassan Ghozlan, *Member, IEEE*, and Gerhard Kramer, *Fellow, IEEE*

Abstract—A waveform channel is considered where the transmitted signal is corrupted by Wiener phase noise and additive white Gaussian noise. A discrete-time channel model that takes into account the effect of filtering on the phase noise is developed. The model is based on a multi-sample receiver, i.e., an integrate-and-dump filter whose output is sampled at a rate higher than the signaling rate. It is shown that, at high Signal-to-Noise Ratio (SNR), the multi-sample receiver achieves a rate that grows logarithmically with the SNR if the number of samples per symbol (oversampling factor) grows with the cubic root of the SNR. Moreover, the pre-log factor is at least 1/2 and can be achieved by amplitude modulation. For an approximate discrete-time model of the multi-sample receiver, the capacity pre-log at high SNR is shown to be at least 3/4 if the number of samples per symbol grows with the square root of the SNR. The analysis shows that phase modulation achieves a pre-log of at least 1/4 while amplitude modulation still achieves a pre-log of 1/2. This is strictly greater than the capacity pre-log of the (approximate) discrete-time Wiener phase noise channel with only one sample per symbol, which is 1/2. Numerical simulations are used to compute lower bounds on the information rates achieved by the multi-sample receiver. The simulations show that oversampling is beneficial for both strong and weak phase noise at high SNR. In fact, the information rates are sometimes substantially larger than when using commonly-used approximate discrete-time models.

Index Terms—Phase noise, Wiener process, waveform channel, capacity, oversampling.

I. INTRODUCTION

Phase noise arises due to the instability of oscillators [1] in communication systems such as satellite communication [2], microwave links [3] or optical fiber communication [4]. The statistical characterization of the phase noise depends on the application. In systems with phase-locked loops (PLL), the residual phase noise follows a Tikhonov distribution [5]. In Digital Video Broadcasting DVB-S2, an example of a satellite communication system, the phase noise process is modeled by

The work of H. Ghazlan was supported by a USC Annenberg Fellowship and the National Science Foundation (NSF) under Grant CCF-09-05235. The work of G. Kramer was supported by an Alexander von Humboldt Professorship endowed by the German Federal Ministry of Education and Research, as well as by the NSF under Grant CCF-09-05235. Part of the material in this paper was presented at the IEEE International Symposium on Information Theory, Istanbul, Turkey, July, 2013, at the Global Communications Conference, Atlanta, GA, December, 2013 and at the IEEE International Symposium on Information Theory, Honolulu, HI, June/July, 2014.

H. Ghazlan was with the Department of Electrical Engineering, University of Southern California, Los Angeles, CA 90089, USA. He is now with Intel Corporation, Hillsboro, OR 97124, USA. (e-mail: hassan.ghozlan@intel.com).

G. Kramer is with the Institute for Communications Engineering, Technical University of Munich, 80333 Munich, Germany (email: gerhard.kramer@tum.de).

Copyright (c) 2014 IEEE. Personal use of this material is permitted. However, permission to use this material for any other purposes must be obtained from the IEEE by sending a request to pubs-permissions@ieee.org.

the sum of the outputs of two infinite-impulse response filters driven by the same white Gaussian noise process [2]. In optical fiber communication, the phase noise in laser oscillators is modeled by a Wiener process [4].

A commonly studied *discrete-time* channel model is

$$Y_k = X_k e^{j\Theta_k} + Z_k \quad (1)$$

where $\{Y_k\}$ are the output symbols, $\{X_k\}$ are the input symbols, $\{\Theta_k\}$ is the phase noise process and $\{Z_k\}$ is additive white Gaussian noise (AWGN). For example, Katz and Shamai [6] studied the model (1) when $\{\Theta_k\}$ is independent and identically distributed (i.i.d.) according to $p_\Theta(\cdot)$, when Θ is uniformly distributed (called a non-coherent AWGN channel) and when Θ has a Tikhonov (or von Mises) distribution (called a partially-coherent AWGN channel). The i.i.d. Tikhonov phase noise models the residual phase error in systems with phase-tracking devices, e.g., phase-locked loops (PLL) and ideal interleavers/deinterleavers. Katz and Shamai [6] characterized some properties of the capacity-achieving distribution. Tight lower bounds on the capacities of memoryless non-coherent and partially coherent AWGN channels were computed by solving an optimization problem numerically in [6] and [7], respectively. Lapidoth studied in [8] a phase noise channel (1) at high SNR. He considered both memoryless phase noise and phase noise with memory. He showed that the capacity grows *logarithmically* with the SNR with a pre-log factor 1/2 if the differential entropy rate of $\{\Theta_k\}$ is finite. The pre-log 1/2 is achieved by amplitude modulation only, and the phase modulation contributes only a bounded number of bits. Dauwels and Loeliger [9] proposed a particle filtering method to compute information rates for discrete-time continuous-state channels with memory and applied the method to (1) for Wiener phase noise and auto-regressive-moving-average (ARMA) phase noise. Barletta, Magarini and Spalvieri [10] computed lower bounds on information rates for (1) with Wiener phase noise by using the auxiliary channel technique proposed in [11] and they computed upper bounds in [12]. They also developed a lower bound based on Kalman filtering in [13]. Barbieri and Colavolpe [14] computed lower bounds with an auxiliary channel slightly different from [10]. Durisi et al. [15], [16] developed capacity bounds for a multi-input multi-output (MIMO) extension of the discrete-time model (1).

A less-studied model since 1990 is the continuous-time model for phase noise channels, also called a *waveform* phase noise channel, see Fig. 1. The received waveform $r(t)$ is

$$r(t) = x(t) e^{j\theta(t)} + n(t), \text{ for } t \in \mathbb{R} \quad (2)$$

where $x(t)$ is the transmitted waveform while $n(t)$ and $\theta(t)$ are additive noise and phase noise, respectively. Continuous-

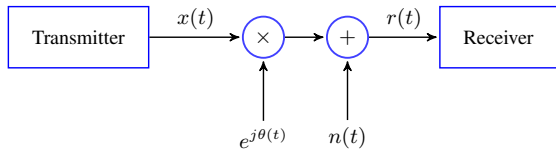


Fig. 1. Waveform phase noise channel.

time *white* phase noise was recently considered in [17, Section IV.C] and [18], [19]. We study the waveform channel (2) with *Wiener* phase noise. A detailed description of the channel is given in Sec. II. This model is reasonable, for example, for optical fiber communication with low to intermediate power and laser phase noise, see [20]–[22]. Since the sampling of a continuous-time Wiener process yields a discrete-time Wiener process (Gaussian random walk), it is tempting to use the model (1) with $\{\Theta\}$ as a discrete-time Wiener process. However, this ignores the effect of *filtering* prior to sampling. It was pointed out in [20] that “even coherent systems relying on amplitude modulation (phase noise is obviously a problem in systems employing phase modulation) will suffer some degradation due to the presence of phase noise”. This is because the filtering converts phase fluctuations to amplitude variations. It is worth mentioning that filtering is necessary before sampling to limit the variance of the noise samples.

The model (1) thus does not fit¹ the channel (2) and it is not obvious whether a pre-log 1/2 is achievable. The model that takes the effect of filtering into account is

$$Y_k = X_k H_k + N_k \quad (3)$$

where $\{H_k\}$ is a fading process. The model (3) falls in the class of non-coherent fading channels, i.e., the transmitter and receiver have knowledge of the distribution of the fading process $\{H_k\}$, but have no knowledge of its realization. For such channels, Lapidoth and Moser showed in [23] that, at high SNR, the capacity grows *double-logarithmically* with the SNR, when the process $\{H_k\}$ is stationary, ergodic and has finite differential entropy rate.

Rather than using a filter and sampling its output at the symbol rate, we use a multi-sample receiver, i.e., a filter whose output is sampled many times per symbol. We show that this receiver achieves a rate that grows *logarithmically* with the SNR if the number of samples per symbol grows with the cubic root of the SNR. Furthermore, we show that a pre-log of 1/2 is achievable through amplitude modulation. We also show for an approximate multi-sample model, where the approximation is to ignore the filtering effect over a sample, that phase modulation contributes 1/4 to the pre-log factor at high SNR if the oversampling factor grows with the square root of SNR. We corroborate the results of the high-SNR analysis with numerical simulations at finite SNR. This paper collects and extends results presented in [24]–[26].

Benefits of oversampling were reported for other problems. For example, in some digital storage systems, it was shown by numerical simulations that oversampling can increase the

information rate [27]. In a low-pass-filter-and-limiter (nonlinear) channel, it was found that oversampling (with a factor of 2) offers a higher information rate [28]. It was demonstrated in [29] that doubling the sampling rate recovers some of the loss in capacity incurred on the bandlimited Gaussian channel with a one-bit output quantizer. For non-coherent block fading channels, it was shown in [30] that by doubling the sampling rate the information rate grows logarithmically at high SNR with a pre-log $1 - 1/N$ rather than $1 - Q/N$ which is the pre-log achieved by sampling at the symbol rate (N is the length of the fading block and Q is the rank of the covariance matrix of the discrete-time channel gains within each block).

This paper is organized as follows. The continuous-time model is described in Sec. II and the discrete-time models of the matched filter receiver and the multi-sample receiver are described in Sec. III. We give a lower bound on the capacity in Sec. IV based on amplitude modulation and show that the pre-log factor is at least 1/2 if the oversampling factor grows with the cubic root of the SNR. We also give a lower bound on the rate achieved by phase modulation for the approximate multi-sample discrete-time model. For such a model, we show that phase modulation contributes at least 1/4 to the pre-log factor, resulting in an overall pre-log factor of 3/4 when both amplitude and phase modulation are used. This is achieved by using an oversampling factor that grows with the square root of the SNR. We develop algorithms to compute tight lower bounds on the information rates of a multi-sample receiver in Sec. V. In Sec. VI, we report the results of numerical simulations which demonstrate the importance of increasing the oversampling factor with the SNR to achieve higher rates. We discuss in Sec. VII our results, related work, open problems and intuitions for our proofs. Finally, we conclude with Sec. VIII.

II. WAVEFORM PHASE NOISE CHANNEL

We use the following notation: $j = \sqrt{-1}$, $*$ denotes the complex conjugate, δ_D is the Dirac delta function, $\lceil \cdot \rceil$ is the ceiling operator. We use X^k as a shorthand for (X_1, X_2, \dots, X_k) . Suppose the transmit-waveform is $x(t)$ and the receiver observes

$$r(t) = x(t) e^{j\theta(t)} + n(t) \quad (4)$$

where $n(t)$ is a realization of a white circularly-symmetric complex Gaussian process $N(t)$ with

$$\begin{aligned} \mathbb{E}[N(t)] &= 0 \\ \mathbb{E}[N(t_1)N^*(t_2)] &= \sigma_N^2 \delta_D(t_2 - t_1). \end{aligned} \quad (5)$$

The phase $\theta(t)$ is a realization of a Wiener process

$$\Theta(t) = \Theta(0) + \int_0^t W(\tau) d\tau \quad (6)$$

where $\Theta(0)$ is uniform on $[-\pi, \pi)$ and $W(t)$ is a real Gaussian process with

$$\begin{aligned} \mathbb{E}[W(t)] &= 0 \\ \mathbb{E}[W(t_1)W(t_2)] &= 2\pi\beta \delta_D(t_2 - t_1) \end{aligned} \quad (7)$$

¹ The model would fit if a very narrow pulse was used as the pulse-shaping filter. Such pulses may be interesting for very large bandwidth applications.

where $0 < \beta < \infty$. The processes $N(t)$ and $\Theta(t)$ are independent of each other and independent of the input. $N_0 = 2\sigma_N^2$ is the single-sided power spectral density of the additive noise. We define $U(t) \equiv \exp(j\Theta(t))$. The auto-correlation function of $U(t)$ is

$$R_U(t_1, t_2) = \mathbb{E}[U(t_1)U^*(t_2)] = \exp(-\pi\beta|t_2 - t_1|) \quad (8)$$

and the power spectral density of $U(t)$ is

$$S_U(f) = \int_{-\infty}^{\infty} R_U(t, t + \tau) e^{-j2\pi f\tau} d\tau = \frac{1}{\pi} \frac{\beta/2}{(\beta/2)^2 + f^2}. \quad (9)$$

The spectrum is said to have a Lorentzian shape. We have $\beta = f_{\text{FWHM}} = 2f_{\text{HWHM}}$ where f_{FWHM} is the full-width at half-maximum and f_{HWHM} is the half-width at half-maximum. One also refers to β as the *linewidth* of the phase noise.

Let T be the transmission interval, then the transmitted waveforms must satisfy the power constraint

$$\mathbb{E} \left[\frac{1}{T} \int_0^T |X(t)|^2 dt \right] \leq \mathcal{P} \quad (10)$$

where $X(t)$ is a random process whose realization is $x(t)$.

III. DISCRETE-TIME MODELS

A. Transmitter

Let (x_1, x_2, \dots, x_b) be the codeword sent by the transmitter. Suppose the transmitter uses a unit-energy pulse $g(t)$ whose time support is $[0, T_s]$ where T_s is the symbol interval, which is finite and fixed. The waveform sent by the transmitter is

$$x(t) = \sum_{m=1}^b x_m g(t - (m-1)T_s). \quad (11)$$

We remark that using pulses that are limited in time to one symbol interval simplifies the analysis because it eliminates intersymbol interference at the receiver. We focus on rectangular pulses for the high SNR analysis in Sec. IV. A disadvantage of a rectangular pulses is the slow decay of the sidelobes in frequency domain, which motivates us to also consider cosine-squared pulses for numerical rate computation in Sec. VI. The sidelobes of a cosine-squared pulses, which is equivalent to a (time-domain) raised-cosine pulse with roll-off factor 1, decay much faster than those of a rectangular pulse. We also remark that Martalò et al [31] extended some of our numerical results for bandlimited pulses. However, their model does not include fully the filtering effects of a continuous-time model.

B. Matched Filter Receiver

The received signal $r(t)$ is fed to a matched filter and the output $y(t)$ of the filter is sampled at the symbol rate as illustrated in Fig. 2. The k -th output sample is

$$\begin{aligned} y_k &= r(t) \star g^*(T_s - t)|_{t=kT_s} \\ &= x_k \int_{-\infty}^{\infty} e^{j\Theta(\tau)} |g(\tau - (k-1)T_s)|^2 d\tau + n_k \end{aligned} \quad (12)$$

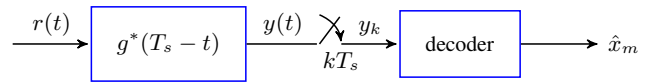


Fig. 2. Matched filter receiver with symbol rate sampling.

where $k = 1, \dots, b$, \star denotes convolution and n_k is the part of the output due to the additive noise. Therefore, we have the discrete-time model

$$Y_k = X_k H_k + N_k \quad (13)$$

where

$$H_k \equiv \int_{-\infty}^{\infty} e^{j\Theta(\tau)} |g(\tau - (k-1)T_s)|^2 d\tau. \quad (14)$$

The transmitter and receiver know the distribution of the fading process $\{H_k\}$ but have no knowledge of its realization. We strongly suspect that $\{H_k\}$ in (14) is stationary, ergodic and has a finite differential entropy rate, i.e., $h(\{H_k\}) > -\infty$. Lapidoth and Moser showed in [23] that, at high SNR, the capacity grows *double-logarithmically* with the SNR under the aforementioned conditions on $\{H_k\}$.

A commonly-used approximation for H_k is

$$\begin{aligned} &\int_{-\infty}^{\infty} e^{j\Theta(\tau)} |g(\tau - (k-1)T_s)|^2 d\tau \\ &\approx e^{j\Theta(kT_s)} \int_{-\infty}^{\infty} |g(\tau - (k-1)T_s)|^2 d\tau \end{aligned} \quad (15)$$

which yields the approximate discrete-time model

$$Y_k = X_k e^{j\Theta(kT_s)} + N_k. \quad (16)$$

We refer to (13) and (16) as the symbol-rate model with filtering and without filtering, respectively. We also refer to (16) as the approximate symbol-rate model. We do not claim that this approximation is always accurate. We introduce the approximate model to examine its validity by comparing it with the discrete-time model based on the multi-sample receiver. We remark that the differential entropy of $\{\Theta(kT_s)\}$ is finite because the linewidth β of $\Theta(t)$ and the symbol interval T_s are finite and therefore, the pre-log of the model (16) is $1/2$.

C. Multi-sample Receiver

Consider next a multi-sample receiver (see Fig. 3). Let L be the number of samples per symbol ($L \geq 1$) and define the sample interval as

$$\Delta = \frac{T_s}{L}. \quad (17)$$

The received waveform $r(t)$ is filtered using an integrator over a sample interval to give the output signal

$$y(t) = \int_{t-\Delta}^t r(\tau) d\tau. \quad (18)$$

The signal $y(t)$ is a realization of a random process $Y(t)$ that is sampled at $t = k\Delta$, $k = 1, \dots, n = bL$. Hence, we have the discrete-time model in which the k -th output sample is

$$Y_k = X_{\lceil k/L \rceil} \Delta e^{j\Theta_k} F_k + N_k \quad (19)$$

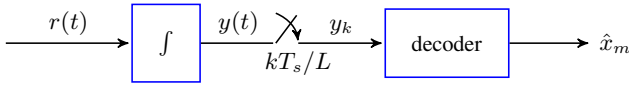


Fig. 3. Multi-sample receiver.

where $Y_k \equiv Y(k\Delta)$, $\Theta_k \equiv \Theta((k-1)\Delta)$,

$$F_k \equiv \frac{1}{\Delta} \int_{(k-1)\Delta}^{k\Delta} g\left(\tau - \left(\left\lfloor \frac{k}{L} \right\rfloor - 1\right) T_s\right) e^{j(\Theta(\tau) - \Theta_k)} d\tau \quad (20)$$

and

$$N_k \equiv \int_{(k-1)\Delta}^{k\Delta} N(\tau) d\tau. \quad (21)$$

The process $\{N_k\}$ is an i.i.d. circularly-symmetric complex Gaussian process with

$$\mathbb{E}[N_k] = 0 \quad (22)$$

$$\mathbb{E}[N_k N_\ell^*] = \sigma_N^2 \Delta \delta_K[l - k] \quad (23)$$

$$\mathbb{E}[N_k N_\ell] = 0 \quad (24)$$

where $\delta_K[\cdot]$ is the Kronecker delta. The process $\{\Theta_k\}$ is the discrete-time Wiener process

$$\Theta_k = \Theta_{k-1} + W_k \quad (25)$$

for $k = 2, \dots, n$, where Θ_1 is uniform on $[-\pi, \pi)$ and $\{W_k\}$ is an i.i.d. real Gaussian process with mean 0 and $\mathbb{E}[|W_k|^2] = 2\pi\beta\Delta$, i.e., the probability density function (pdf) of W_k is $p_{W_k}(w) = G(w; 0, \sigma_W^2)$ where

$$G(w; \mu, \sigma^2) = \frac{1}{\sqrt{2\pi\sigma^2}} \exp\left(-\frac{(w - \mu)^2}{2\sigma^2}\right) \quad (26)$$

and $\sigma_W^2 = 2\pi\beta\Delta$. The random variable $(W_k \bmod 2\pi)$ is a *wrapped Gaussian* and its pdf is

$$p_W(w; \sigma^2) = \sum_{i=-\infty}^{\infty} G(w - 2i\pi; 0, \sigma^2). \quad (27)$$

Moreover, $\{F_k\}$ and $\{W_k\}$ are independent of $\{N_k\}$ but not independent of each other. Equations (10) and (11) imply the power constraint

$$\frac{1}{b} \sum_{m=1}^b \mathbb{E}[|X_m|^2] \leq P \equiv \mathcal{P}T_s. \quad (28)$$

The signal-to-noise ratio SNR is defined as

$$\text{SNR} \equiv \frac{P}{\sigma_N^2 T_s} = \frac{\mathcal{P}}{\sigma_N^2}. \quad (29)$$

D. Information Rates

We use \mathbf{Y}^k as a shorthand for $(\mathbf{Y}_1, \mathbf{Y}_2, \dots, \mathbf{Y}_k)$ where

$$\mathbf{Y}_k \equiv (Y_{(k-1)L+1}, Y_{(k-1)L+2}, \dots, Y_{(k-1)L+L}). \quad (30)$$

The capacity of a point-to-point channel is given by

$$C(\text{SNR}) = \lim_{b \rightarrow \infty} \frac{1}{b} \sup I(X^b; \mathbf{Y}^b) \quad (31)$$

where the supremum is over all joint distributions of the input symbols satisfying the power constraint. For a given input distribution, the achievable rate R is

$$R(\text{SNR}) = I(X; Y) \equiv \lim_{b \rightarrow \infty} \frac{1}{b} I(X^b; \mathbf{Y}^b). \quad (32)$$

IV. HIGH-SNR INFORMATION RATES

In this section, we study rectangular pulses, i.e., we consider

$$g(t) \equiv \begin{cases} \sqrt{1/T_s}, & 0 \leq t < T_s, \\ 0, & \text{otherwise.} \end{cases} \quad (33)$$

It follows that F_k in (20) becomes

$$F_k \equiv \frac{1}{\Delta} \int_{(k-1)\Delta}^{k\Delta} e^{j(\Theta(\tau) - \Theta_k)} d\tau. \quad (34)$$

We define $X_A \equiv |X|$ and $\Phi_X \equiv \arg(X)$ where $\arg(\cdot)$ denotes the phase angle (also called the argument) of a complex number. We decompose the mutual information using the chain rule into two parts:

$$I(X^b; \mathbf{Y}^b) = I(X_A^b; \mathbf{Y}^b) + I(\Phi_X^b; \mathbf{Y}^b | X_A^b) \quad (35)$$

where $X_A^b = (|X_1|, \dots, |X_b|)$ and $\Phi_X^b = (\arg X_1, \dots, \arg X_b)$. Define

$$I(X_A; Y) \equiv \lim_{b \rightarrow \infty} \frac{1}{b} I(X_A^b; \mathbf{Y}^b) \quad (36)$$

and

$$I(\Phi_X; Y | X_A) \equiv \lim_{b \rightarrow \infty} \frac{1}{b} I(\Phi_X^b; \mathbf{Y}^b | X_A^b). \quad (37)$$

It follows from (32)–(37) that

$$I(X; Y) = I(X_A; Y) + I(\Phi_X; Y | X_A). \quad (38)$$

The first term represents the contribution of the amplitude modulation while the second term represents the contribution of the phase modulation. The results of this section are summarized in Theorem 1 and Theorem 2 which address the contribution of amplitude modulation and phase modulation to the information rate, respectively.

Before we proceed to the theorems, we introduce an important result that we use multiple times in the paper. Let X and Y be the input and output of a channel, respectively and let $q(\cdot|\cdot)$ be a valid conditional pdf, which represents an ‘‘auxiliary channel’’. The following auxiliary-channel lower bound holds:

$$I(X; Y) \geq \underline{I}(X; Y) = \mathbb{E}[\log q_{Y|X}(Y|X) - \log q_Y(Y)] \quad (39)$$

where $q_Y(\cdot)$ is the output pdf obtained by connecting the true input source to the auxiliary channel. Note that $\mathbb{E}[\cdot]$ is the expectation according to the *true* distribution of X and Y . The lower bound is the rate achieved by a mismatched decoder. See [32, pp. 6-7] for a recent comprehensive review on mismatched decoding.

Theorem 1 (Amplitude Modulation): Consider the discrete-time model in (19) with F_k as defined in (34). If $L = \lceil \sqrt[3]{(\beta T_s)^2 \text{SNR}} \rceil$ and the process $\{X_k\}$ is i.i.d. such that

$(|X_k|^2 - P/2)$ is exponentially distributed with mean $P/2$, then

$$\lim_{\text{SNR} \rightarrow \infty} I(X_A; Y) - \frac{1}{2} \log \text{SNR} \geq -2 - \frac{1}{2} \log(8\pi) - \frac{\pi^2}{45}. \quad (40)$$

Proof: See Appendix A. The lower bound in (40) is achieved by the double-filtering receiver structure shown in Fig. 4. We borrow the term ‘‘double-filtering’’ from [20]. ■

Theorem 1 implies that the capacity pre-log satisfies

$$\lim_{\text{SNR} \rightarrow \infty} \frac{C(\text{SNR})}{\log \text{SNR}} \geq \frac{1}{2} \quad (41)$$

which follows from (40) and $C(\text{SNR}) \geq I(X; Y) \geq I(X_A; Y)$. The capacity thus grows logarithmically at high SNR with a pre-log factor of at least $1/2$ if the oversampling factor L grows with the cubic root of SNR.

Consider next a simplified model that does not include the effect of filtering modeled by $\{F_k\}$. More specifically, the k th output of the simplified approximate model is

$$\Psi_k = X_{\lceil k/L \rceil} \Delta e^{j\Theta_k} + N_k \quad (42)$$

where X_k is k th input symbol and $\{\Theta_k\}$ and $\{N_k\}$ are the same processes defined in Sec. III-C.

Theorem 2 (Phase Modulation): Consider the discrete-time model in (42). If $L = \lceil \sqrt{\pi\beta T_s \text{SNR}/2} \rceil$ and the input X^b is i.i.d. with $\arg(X_k)$ independent of $|X_k|$ for $k = 1, \dots, b$ such that $\arg(X_k)$ is uniformly distributed over $[-\pi, \pi)$ and $(|X_k|^2 - P/2)$ is exponentially distributed with mean $P/2$, then

$$\lim_{\text{SNR} \rightarrow \infty} I(X_A; \Psi) - \frac{1}{2} \log \text{SNR} \geq -2 - \frac{1}{2} \log(8\pi) \quad (43)$$

and

$$\lim_{\text{SNR} \rightarrow \infty} I(\Phi_X; \Psi|X_A) - \frac{1}{4} \log \text{SNR} \geq -\frac{1}{4} \log(64\pi\beta T_s) - \frac{1}{2}. \quad (44)$$

Proof: See Appendix B. The lower bounds (43) and (44) are achieved by the receiver structure shown in Fig. 5. ■

Theorem 2 implies that the capacity pre-log for the approximate model (42) satisfies

$$\lim_{\text{SNR} \rightarrow \infty} \frac{C(\text{SNR})}{\log \text{SNR}} \geq \frac{3}{4} \quad (45)$$

which follows from (43)-(44) by using $C(\text{SNR}) \geq I(X; \Psi) = I(X_A; \Psi) + I(\Phi_X; \Psi|X_A)$. This shows that the capacity grows logarithmically at high SNR with a pre-log factor of at least $3/4$. We remark that Barletta and Kramer [33] extended the result of Theorem 2 to the full model (19) that includes the filtering effect, i.e., they showed that $C(\text{SNR}) \geq 3/4$ for (19) if $L = \lceil \sqrt{\text{SNR}} \rceil$. More generally, for $L = \lceil \text{SNR}^\alpha \rceil$, they showed for the full model that

$$\lim_{\text{SNR} \rightarrow \infty} \frac{C(\text{SNR})}{\log(\text{SNR})} \geq \begin{cases} 2\alpha, & 0 < \alpha \leq 1/3 \\ (1 + \alpha)/2, & 1/3 \leq \alpha \leq 1/2 \\ 3/4, & 1/2 \leq \alpha < 1. \end{cases} \quad (46)$$

V. RATE COMPUTATION AT FINITE SNR

We develop algorithms to compute the information rate numerically. We use X_k to denote the k th input *sample* which is defined by

$$X_k = X_{\lceil k/L \rceil} g((k \bmod L)\Delta). \quad (47)$$

The information rate $I(X; Y)$ in (32) can be expressed as

$$I(X; Y) = \lim_{b \rightarrow \infty} \frac{1}{b} I(X^b; Y^b) \quad (48)$$

which follows from (47) and (30). One difficulty in evaluating (48) is that the joint distribution of $\{F_k\}$ and $\{W_k\}$ is not available in closed form. Even the distribution of F_k is not available in closed form (there is an approximation for small linewidth, see (16) in [21]). However, we can numerically compute tight lower bounds on $I(X; Y)$ by using the auxiliary-channel technique (cf. (39)). We use the following algorithm [11].

- 1) Sample a long sequence (x^n, y^n) according to the *true* joint distribution of X^n and Y^n ;
- 2) Compute $q_{Y^n|X^n}(y^n|x^n)$ and

$$q_{Y^n}(y^n) = \sum_{\tilde{x}^n} p_{X^n}(\tilde{x}^n) q_{Y^n|X^n}(y^n|\tilde{x}^n) \quad (49)$$

where p_{X^n} is the true distribution of X^n ;

- 3) Estimate $\underline{I}(X; Y)$ using

$$\underline{I}(X; Y) \approx \frac{1}{b} \log \left(\frac{q_{Y^n|X^n}(y^n|x^n)}{q_{Y^n}(y^n)} \right). \quad (50)$$

Auxiliary Channel I: Consider the auxiliary channel

$$\Psi_k = X_k \Delta e^{j\Theta_k} + N_k \quad (51)$$

where $\{\Theta_k\}$ and $\{N_k\}$ are defined in Sec. III-C and X_k is defined by (47). The channel output Ψ is the same as Y in (19) *except* that F_k is replaced by 1 or more generally with $g((k \bmod L)\Delta)$. The channel is described by the conditional distribution

$$p_{\Psi^n|X^n}(y^n|x^n) = \int_{\theta^n} p_{\Theta^n, \Psi^n|X^n}(\theta^n, y^n|x^n) d\theta^n \quad (52)$$

where

$$\begin{aligned} p_{\Theta^n, \Psi^n|X^n}(\theta^n, y^n|x^n) \\ = \prod_{k=1}^n p_{\Theta_k|\Theta_{k-1}}(\theta_k|\theta_{k-1}) p_{\Psi|X, \Theta}(y_k|x_k, \theta_k) \end{aligned} \quad (53)$$

with

$$p_{\Theta_k|\Theta_{k-1}}(\theta|\tilde{\theta}) = \begin{cases} p_W(\theta - \tilde{\theta}; \sigma_W^2), & k \geq 2 \\ 1/(2\pi), & k = 1 \end{cases} \quad (54)$$

and

$$p_{\Psi|X, \Theta}(y|x, \theta) = \frac{1}{\pi\sigma_N^2\Delta} \exp\left(-\frac{|y - x\Delta e^{j\theta}|^2}{\sigma_N^2\Delta}\right). \quad (55)$$

The channel $p_{\Psi^n|X^n}$ has continuous states θ^n , which implies that step 2 of the algorithm can not be computed directly. To compute the integrals, we quantize the states (the phase noise). Finer quantization results in more accurate results

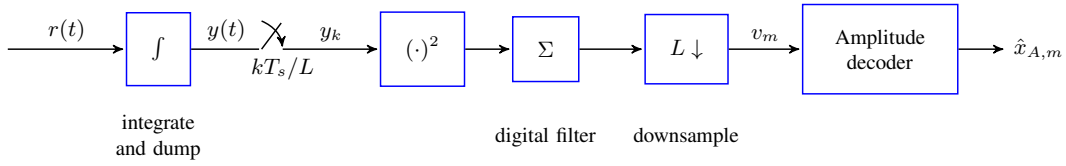


Fig. 4. Double filtering receiver.

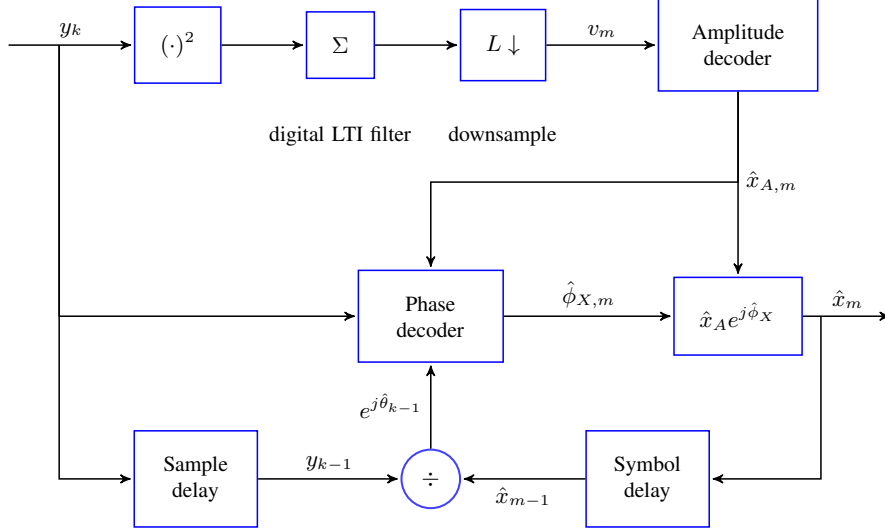


Fig. 5. Two-stage decoding in a multi-sample receiver. The upper branch is part of the double filtering receiver for amplitude decoding. The lower branch is a phase-noise tracker which outputs an estimate $\hat{\theta}_{k-1}$ of the phase noise where $\hat{\theta}_{k-1} = \arg(y_{k-1}/\hat{x}_{m-1})$ where $m = \lceil k/L \rceil$ (cf. (157)). The phase decoder uses the estimate of the phase noise $\hat{\theta}_{k-1}$ and the estimated amplitude $\hat{x}_{A,m}$ to produce an estimate $\hat{\phi}_{X,m}$ of the phase of x_m .

but is also more computationally intensive. We approach this issue by first computing an estimate of the rate at a small number of quantization levels, then we increase the number of quantization levels as long as there is a significant difference between the estimated rates. When there is no significant change in the rate estimates, we take that to be a (lower bound on the) rate with the auxiliary channel Ψ_k . This approach is demonstrated in Fig. 8 and Fig. 9, both in Sec. VI. However, in Fig. 10 and Fig. 11, we show only the final result after finding the appropriate number of quantization levels. Next, we describe formally the quantization of the states and the rate computation in that case.

Auxiliary Channel II: We use the following auxiliary channel for the numerical simulations:

$$\Upsilon_k = \mathbf{X}_k \Delta e^{jS_k} + N_k. \quad (56)$$

The conditional probability is

$$p_{\Upsilon^n | \mathbf{X}^n}(y^n | x^n) = \sum_{s^n \in \mathcal{S}^n} p_{S^n, \Upsilon^n | \mathbf{X}^n}(s^n, y^n | x^n) \quad (57)$$

where \mathcal{S} is a finite set and

$$\begin{aligned} & p_{S^n, \Upsilon^n | \mathbf{X}^n}(s^n, y^n | x^n) \\ &= \prod_{k=1}^n p_{S_k | S_{k-1}}(s_k | s_{k-1}) p_{\Psi | \mathbf{X}, \Theta}(y_k | x_k, s_k) \end{aligned} \quad (58)$$

where

$$p_{S_k | S_{k-1}}(s | \tilde{s}) = \begin{cases} Q(s | \tilde{s}), & k \geq 2 \\ 1/|\mathcal{S}|, & k = 1. \end{cases} \quad (59)$$

Next, we describe our choice of \mathcal{S} and $Q(\cdot | \cdot)$. We partition $[-\pi, \pi)$ into S intervals with equal lengths and pick the mid points of these intervals to be the elements of \mathcal{S} , i.e., we have

$$\mathcal{S} = \{\hat{s}_i : i = 1, \dots, S\} \text{ where } \hat{s}_i = i \frac{2\pi}{S} - \frac{\pi}{S} - \pi. \quad (60)$$

The state transition probability $Q(\cdot | \cdot)$ is chosen similar to [10] and [12]:

$$Q(s | \tilde{s}) = \frac{2\pi}{S} \int_{(\phi, \tilde{\phi}) \in \mathcal{R}(s) \times \mathcal{R}(\tilde{s})} p_W(\phi - \tilde{\phi}; \sigma_W^2) d\phi d\tilde{\phi} \quad (61)$$

where $\mathcal{R}(s) = [s - \pi/S, s + \pi/S)$, i.e., $\mathcal{R}(s)$ is the interval whose midpoint is s . The larger S and L are, the better the auxiliary channel (56) approximates the actual channel (19). We remark that the auxiliary channel gives a *valid* lower bound on $I(X; Y)$ even for small S and L .

A. Computing The Conditional Probability

Suppose the input \mathbf{X}^n has the distribution $p_{\mathbf{X}^n}$. A Bayesian network for $\mathbf{X}^n, S^n, \Upsilon^n$ is shown in Fig. 6. The probability $p_{\Upsilon^n | \mathbf{X}^n}(y^n | x^n)$ can be computed using

$$p_{\Upsilon^n | \mathbf{X}^n}(y^n | x^n) = \sum_{s \in \mathcal{S}} \rho_n(s) \quad (62)$$

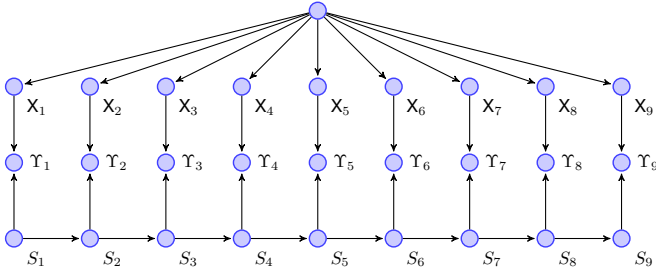


Fig. 6. Bayesian network for $\mathbf{X}^n, \mathbf{S}^n, \mathbf{Y}^n$ for $n = 9$.

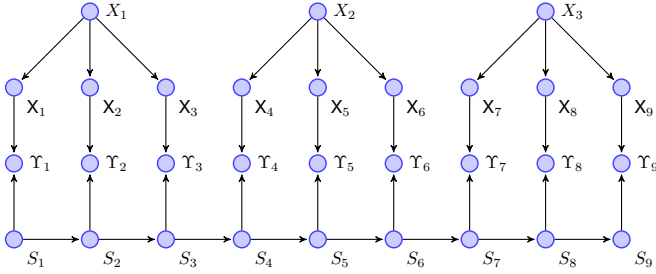


Fig. 7. Bayesian network for $\mathbf{X}^n, \mathbf{S}^n, \mathbf{Y}^n$ for $n = 9$ and $L = 3$.

where we recursively compute

$$\begin{aligned} \rho_k(s) &\equiv p_{S_k, \Upsilon^k | \mathbf{X}^n}(s, y^k | x^n) \\ &\stackrel{(a)}{=} \sum_{\tilde{s} \in \mathcal{S}} p_{S_{k-1}, S_k, \Upsilon^k | \mathbf{X}^n}(\tilde{s}, s, y^k | x^n) \\ &\stackrel{(b)}{=} \sum_{\tilde{s} \in \mathcal{S}} \rho_{k-1}(\tilde{s}) p_{S_k, \Upsilon^k | S_{k-1}, \Upsilon^{k-1}, \mathbf{X}^n}(s, y_k | \tilde{s}, y^{k-1}, x^n) \\ &= \sum_{\tilde{s} \in \mathcal{S}} \rho_{k-1}(\tilde{s}) Q(s | \tilde{s}) p_{\Psi | \mathbf{X}, \Theta}(y_k | x_k, s) \end{aligned} \quad (63)$$

with the initial value $\rho_0(s) = 1/|\mathcal{S}|$. Step (a) is a marginalization, (b) follows from Bayes' rule and the definition of ρ_k in (63), while (64) follows from the structure of Fig. 6. We remark that (64) is the same as with independent X_1, \dots, X_n , e.g., see equation (9) in [34, Sec. IV].

B. Computing The Marginal Probability

Define $\mathbf{X}_m \equiv (X_{(m-1)L+1}, X_{(m-1)L+2}, \dots, X_{(m-1)L+L})$. Suppose the input symbols are i.i.d. and $X_m \in \mathcal{X}$ where \mathcal{X} is a finite set. Therefore, $p_{\mathbf{X}^n}$ has the form

$$p_{\mathbf{X}^n}(x^n) = \prod_{m=1}^b p_{\mathbf{X}}(\mathbf{X}_m). \quad (65)$$

A Bayesian network for $\mathbf{X}^n, \mathbf{S}^n, \mathbf{Y}^n$ is shown in Fig. 7. The probability $p_{\Upsilon^n}(y^n)$ can be computed using

$$p_{\Upsilon^n}(y^n) = \sum_{s \in \mathcal{S}} \psi_b(s) \quad (66)$$

where $\psi_m(s) \equiv p_{S_{mL}, \mathbf{Y}^m}(s, \mathbf{y}^m)$ which can be computed using the recursion:

$$\begin{aligned} \psi_m(s) &= \sum_{\tilde{\mathbf{x}} \in \mathcal{X}_L} p_{\mathbf{X}}(\tilde{\mathbf{x}}) \sum_{\tilde{s} \in \mathcal{S}} \psi_{m-1}(\tilde{s}) p_{S_{mL}, \mathbf{Y}^m | S_{(m-1)L}, \mathbf{X}_m}(s, \mathbf{y}_m | \tilde{s}, \tilde{\mathbf{x}}) \end{aligned} \quad (67)$$

with the initial value $\psi_0(s) = 1/|\mathcal{S}|$. The set \mathcal{X}_L is

$$\mathcal{X}_L = \{x \cdot (g(\Delta), g(2\Delta), \dots, g(L\Delta)) : x \in \mathcal{X}\}. \quad (68)$$

We remark that $|\mathcal{X}_L| = |\mathcal{X}|$ and not $|\mathcal{X}|^L$. Next, we define

$$\chi_{m,L}(s, \tilde{s}, \tilde{\mathbf{x}}) = p_{S_{mL}, \mathbf{Y}^m | S_{(m-1)L}, \mathbf{X}_m}(s, \mathbf{y}_m | \tilde{s}, \tilde{\mathbf{x}}) \quad (69)$$

for $s, \tilde{s} \in \mathcal{S}$ and $\tilde{\mathbf{x}} \in \mathcal{X}_L$. Computing $\chi_{m,L}(s, \tilde{s}, \tilde{\mathbf{x}})$ is similar to computing ρ_n (see (64)). Intuitively, this is because a block of L samples in Fig. 7 has a structure similar to Fig. 6. More precisely, $\chi_{m,L}(s, \tilde{s}, \tilde{\mathbf{x}})$ can be computed recursively by using

$$\begin{aligned} \chi_{m,\ell}(s, \tilde{s}, \tilde{\mathbf{x}}) &= \sum_{\varsigma \in \mathcal{S}} \chi_{m,\ell-1}(\varsigma, \tilde{s}, \tilde{\mathbf{x}}) Q(s | \varsigma) p_{\Psi | \mathbf{X}, \Theta}(y_{(m-1)L+\ell} | \tilde{x}_\ell, \varsigma) \end{aligned} \quad (70)$$

with the initial value

$$\chi_{m,0}(s, \tilde{s}, \tilde{\mathbf{x}}) = \begin{cases} 1, & s = \tilde{s} \\ 0, & \text{otherwise.} \end{cases} \quad (71)$$

Therefore, computing $p_{\Upsilon^n}(y^n)$ involves two levels of recursion: 1) a recursion over the symbols as described by (67) and 2) a recursion over the samples within a symbol as described by (70).

VI. NUMERICAL SIMULATIONS

We use two pulses with a symbol-interval time support:

- A unit-energy square pulse

$$g_1(t) = \frac{1}{\sqrt{T_s}} \text{rect}\left(\frac{t}{T_s}\right) \quad (72)$$

where

$$\text{rect}(t) \equiv \begin{cases} 1, & |t| \leq 1/2, \\ 0, & \text{otherwise.} \end{cases} \quad (73)$$

- A unit-energy cosine-squared pulse

$$g_2(t) = \frac{1}{\sqrt{T_s/2}} \cos^2\left(\frac{\pi t}{T_s}\right) \text{rect}\left(\frac{t}{T_s}\right). \quad (74)$$

The first step of the algorithm is to sample a long sequence according to the true joint distribution of \mathbf{X}^n and \mathbf{Y}^n . To generate samples according to the original channel (19), we must accurately represent digitally the continuous-time waveform (4). We use a simulation oversampling rate $L_{\text{sim}} = 1024$ samples/symbol. After the filter (18), the receiver has L samples/symbol distributed according to (19). Next, to choose a proper sequence length, we follow the approach suggested in [11]: for a candidate length, run the algorithm about 10 times (each with a new random seed) and check whether all estimates of the information rate agree up to the desired accuracy. We used $b = 10^4$ unless otherwise stated.

For efficient implementation of (64), $p_{\Psi | \mathbf{X}, \Theta}(\cdot | \cdot, \cdot)$ can be factored out of the summation to yield:

$$\rho_k(s) = p_{\Psi | \mathbf{X}, \Theta}(y_k | x_k, s) \overbrace{\sum_{\tilde{s} \in \mathcal{S}} \rho_{k-1}(\tilde{s}) Q(s | \tilde{s})}^{\rho'_k(s)}. \quad (75)$$

Moreover, since $Q(\cdot | \cdot)$ can be represented by a circulant matrix due to symmetry, $\rho'_k(\cdot)$ can be computed efficiently using the Fast Fourier Transform (FFT). Similarly, the computation of (70) can be done efficiently by factoring out $p_{\Psi | \mathbf{X}, \Theta}(\cdot | \cdot, \cdot)$ and by using the FFT.

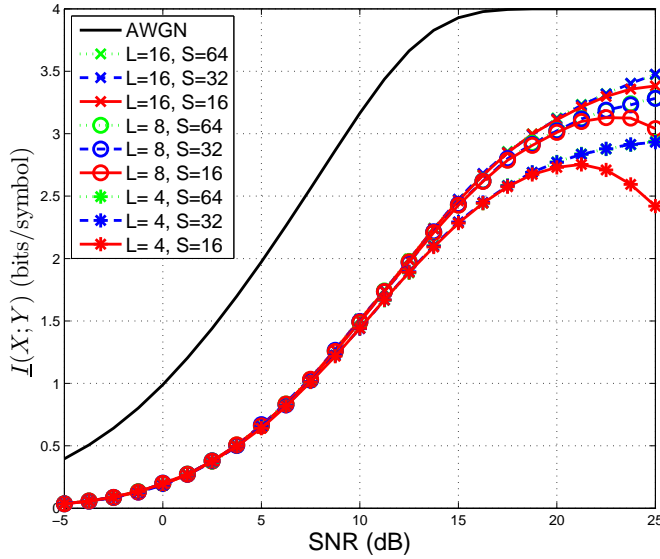


Fig. 8. Lower bounds on rates for 16-QAM, square transmit-pulse and multi-sample receiver at $f_{\text{HWHM}}T_s = 0.125$.

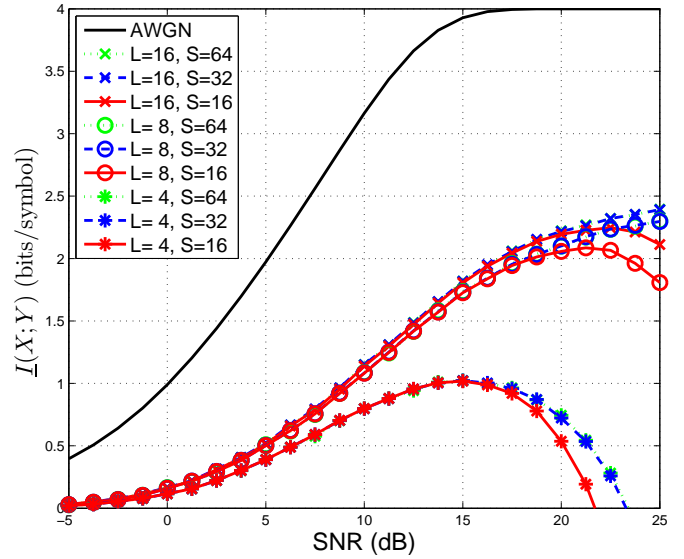


Fig. 9. Lower bounds on rates for 16-QAM, cosine-squared transmit-pulse and multi-sample receiver at $f_{\text{HWHM}}T_s = 0.125$.

A. Very Large Linewidth

Suppose $f_{\text{HWHM}}T_s = 0.125$ and the input symbols are independently and uniformly distributed (i.u.d.) 16-QAM. Fig. 8 shows an estimate of $\underline{I}(X;Y)$ for a square transmit-pulse, i.e., $g(t) = g_1(t - T_s/2)$ and an L -sample receiver with $L = 4, 8, 16$ and $S = 16, 32, 64$. The curves with $S = 64$ are indistinguishable from the curves with $S = 32$ over the entire SNR range for all values of L , and hence it seems that $S = 32$ is adequate up to 25 dB. Even $S = 16$ seems to be adequate up to 20 dB. We remark that the non-monotonicity of some lower bounds is an artifact of the auxiliary channel being “far” from the true channel, specifically because the number S of quantization levels of Auxiliary Channel II is too low for some SNR values. The important trend in Fig. 8 is that higher oversampling rate L is needed at high SNR to extract all the information from the received signal. For example, $L = 4$ suffices up to $\text{SNR} \sim 10$ dB, $L = 8$ suffices up to $\text{SNR} \sim 15$ dB but $L \geq 16$ is needed beyond that. It was pointed out in [11] that the lower bounds can be interpreted as the information rates achieved by mismatched decoding. For example, $\underline{I}(X;Y)$ for $L = 8$ and $S \geq 32$ in Fig. 8 is essentially the information rate achieved by a multi-sample (8-sample) receiver that uses maximum-likelihood decoding for the simplified channel (51) when it is operated in the original channel (19).

Fig. 9 shows an estimate of $\underline{I}(X;Y)$ for a cosine-squared transmit-pulse, i.e., $g(t) = g_2(t - T_s/2)$ and an L -sample receiver at $L = 4, 8, 16$ and $S = 16, 32, 64$. We find that $S = 32$ suffices up to ~ 25 dB. We see in Fig. 9 the same trend as in Fig. 8: higher L is needed at higher SNR. Furthermore, the square pulse is better than the cosine-squared pulse for the same oversampling rate L . It might seem strange that the cosine-squared pulse curves are substantially lower than the square pulse curves despite taking into account the pulse shape in the auxiliary channel model, see (56) and (47). One obtains

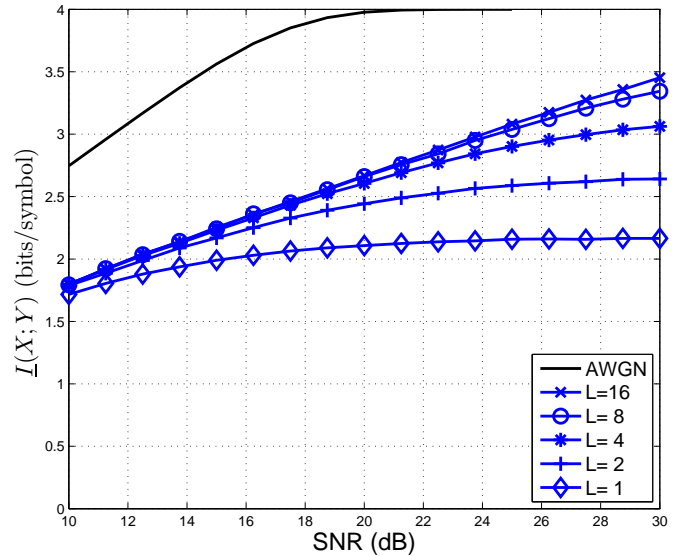


Fig. 10. Lower bounds on rates for 16-PSK, square transmit-pulse and multi-sample receiver at $f_{\text{HWHM}}T_s = 0.0125$.

insight on this effect with the following Gedankenexperiment. Suppose we use a pulse that is narrow and peaky in time. Then an integrate-and-dump receiver with oversampling puts out essentially only one useful sample per symbol. One may as well, therefore, use only one sample per symbol.

B. Large Linewidth

As the linewidth decreases, the benefit of oversampling at the receiver becomes apparent only at higher SNR. For example, for $f_{\text{HWHM}}T_s = 0.0125$ and i.u.d. 16-PSK input, Fig. 10 shows an estimate of $\underline{I}(X;Y)$ for a square transmit-pulse and an L -sample receiver at $L = 1, 2, 4, 8, 16$ and $S = 64$. We see that $L = 4$ suffices up to $\text{SNR} \sim 19$ dB, $L = 8$ suffices up to $\text{SNR} \sim 24$ dB and only beyond that $L \geq 16$ is necessary.

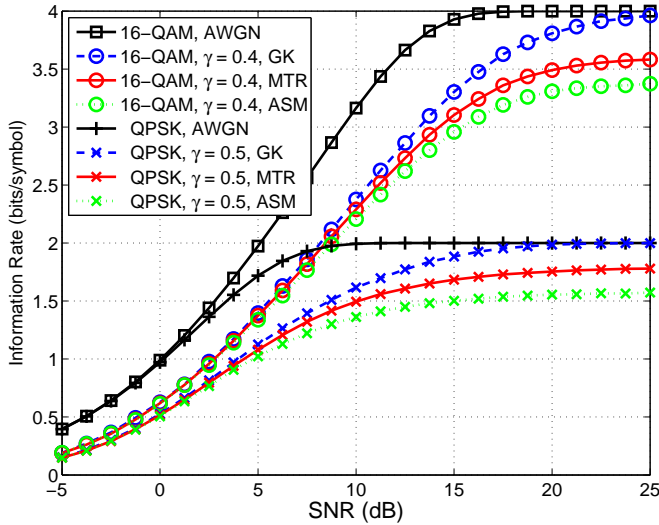


Fig. 11. Comparison of information rates for different models.

We conclude from Fig. 8–10 that the required L depends on 1) the linewidth f_{FWHM} of the phase noise; 2) the pulse $g(t)$; and 3) the SNR.

C. Comparison With Other Models

We compare the discrete-time model of the multi-sample receiver with other discrete-time models. The simulation parameters for our model (labeled GK) are $b = 10^4$, $L = 16$ (with $L_{\text{sim}} = 1024$) and $S = 64$ for 16-QAM ($S = 128$ was too computationally intensive) and $S = 128$ for QPSK. We set $\gamma^2 = 2\pi\beta T_s$. In Fig. 11, we show curves for the approximate symbol-rate model (16), which are labeled ASM. The simulation parameters for this model are $b = 10^5$ and $S = 128$.

We also show curves for the Martalò-Tripodi-Raheli (MTR) model [34] in Fig. 11. For the sake of comparison, we adapt the model in [34] from a square-root raised-cosine pulse to a square pulse and write the “matched” filter output $\{V_m\}$ as

$$V_m = \sum_{\ell=1}^{L_{\text{sim}}} \Psi_{(m-1)L+\ell} \quad (76)$$

where $m = 1, \dots, b$ and Ψ_k is defined in (51). The auxiliary channel is

$$Y_m = X_m e^{j\Theta_m} + Z_m, \quad m \geq 1 \quad (77)$$

where the process $\{Z_m\}$ is an i.i.d. circularly-symmetric complex Gaussian process with mean 0 and $\mathbb{E}[|Z_m|^2] = \sigma_N^2 T_s$ while the process $\{\Theta_m\}$ is a first-order Markov process (not a Wiener process) with a time-invariant transition probability, i.e., for $k \geq 2$ and all $\theta_k, \theta_{k-1} \in [-\pi, \pi)$, we have $p_{\Theta_k|\Theta_{k-1}}(\theta_k|\theta_{k-1}) = p_{\Theta_2|\Theta_1}(\theta_k|\theta_{k-1})$. Furthermore, the phase space is quantized to a finite number S of states and the transition probabilities are estimated by means of simulation. The probabilities are then used to compute a lower bound on the information rate. The simulation parameters for the MTR model are $b = 10^5$, $L_{\text{sim}} = 16$ and $S = 128$.

We point out that MTR rates are essentially achievable rates for the symbol-rate model with filtering (13) that are valid up to some SNR that grows with the oversampling rate. We observe from Fig. 11 the following:

- 1) The rates of ASM and MTR saturate well below the rate achieved by the multi-sample receiver, which implies that symbol-rate sampling results in information loss at high SNR.
- 2) The multi-sample receiver rates are indistinguishable from the MTR rates at low SNR which implies that matched filtering with symbol-rate sampling incurs practically no information loss, i.e., using (16) to compute rates at low/moderate SNR gives accurate results.
- 3) MTR is indistinguishable from ASM at low SNR which implies that approximating (13) as (16) can be justified at low SNR, i.e., the filtering effect may be ignored.

We remark that the saturation at high SNR of the rates of the symbol-rate models at a value lower than the entropy of the source should not be surprising. The impact of the additive noise is smaller at high SNR, but the effect of phase noise and/or filtering are not necessarily reduced. For example, consider the memoryless channel $Y = HX + Z$ and a fixed-size constellation (e.g. M -QAM). We have the following upper bound (by using a genie-aided argument)

$$\begin{aligned} I(X; Y) &\leq I(X; YZ) \\ &= H(X) - H(X|HX). \end{aligned} \quad (78)$$

The term $H(X|HX)$ represents impact of the ambiguity due to the randomness of H . For the special case of $Y = e^{j\Theta}X + Z$, we have

$$I(X; Y) \leq H(X) - H(\Phi_X|\Phi_X + \Theta) \quad (79)$$

i.e., one may fully recover the amplitude of X but not the phase of X because of the ambiguity due to Θ . Moreover, for $Y = e^{j\Theta}X + Z$, there is a more general upper bound on the contribution of phase modulation given by

$$\begin{aligned} I(\Phi_X; Y|X_A) &\leq I(\Phi_X; Y|X_A, Z) \\ &= I(\Phi_X; \Phi_X + \Theta|X_A) \\ &= h(\Phi_X + \Theta|X_A) - h(\Theta) \\ &\leq \log(2\pi) - h(\Theta) \end{aligned} \quad (80)$$

This upper bound is more general than the earlier one in the sense that it is valid for any input constellation (of any size). Unfortunately, we do not have a simple upper bound expression similar to $\log(2\pi) - h(\Theta)$ to predict the cap on the information rate for the multi-sample receiver. Obtaining such an upper bound is beyond the scope of this paper.

VII. DISCUSSION

1) The authors of [21] treated on-off keying in the presence of Wiener phase noise by using a double-filtering receiver, which is composed of an intermediate frequency (IF) filter, followed by an envelope detector (square-law device) and then a post-detection filter. They showed that by optimizing the IF receiver bandwidth the double-filtering receiver outperforms the single-filtering (matched filter) receiver. Furthermore, they showed

via simulation that the optimum IF bandwidth increases with the SNR. This is similar to our result in the sense that we require the number of samples per symbol to increase with the SNR in order to achieve a rate that grows logarithmically with the SNR. We remark that Dallal and Shamai [35] derived an upper bound on the error probability of (a variant of) the double filtering receiver for systems employing noncoherent demodulation, such as frequency shift keying (FSK), on-off keying (OOK) and pulse-position modulation (PPM). Relevant analysis can be found in [36], [37] and references therein. The analysis typically involves moments of filtered Wiener phase noise.

2) The phase modulation pre-log of 1/4 in (44) requires only 2 samples per symbol for which the time resolution $1/\Delta$ grows as the square root of the SNR. In other words, one does not need an analog-to-digital converter (ADC) with sampling every T_s/L seconds. Instead, one may use two ADCs that sample every T_s seconds and the sampling instants are offset by T_s/L seconds. For large L , two ADCs with low sampling rate would be less complex than one ADC with a very high sampling rate. It is interesting to contemplate whether another receiver, e.g., a non-coherent receiver, can achieve the maximum amplitude modulation pre-log of 1/2 but requires only 1 sample per symbol. If so, one would need only 3 samples per symbol to achieve a pre-log of 3/4.

3) The paper [24] shows that a pre-log of 1/2 is achievable for the model (19) when $L \propto \sqrt{\text{SNR}}$. Theorem 1 implies that a pre-log of 1/2 can be achieved using $L \propto \sqrt[3]{\text{SNR}}$ and this perhaps can be reduced further. But using $L \propto \sqrt{\text{SNR}}$ may simplify the receiver design. Specifically, the amplitude decoder designed for the auxiliary channel in [24] can be used for any phase noise linewidth β because the auxiliary channel is (99) with $\tilde{G} = 1$ which is independent of β . In contrast, using $L = \sqrt[3]{\beta^2 \text{SNR}}$ requires different amplitude decoders for different linewidths because the auxiliary channel in this case is (99) with $\tilde{G} = \mathbb{E}[G]$ which depends on β .

4) For the multi-sample approximate model (42), Barletta and Kramer [38] derived an upper bound on the rate and showed that if

$$L = \lceil \text{SNR}^\alpha \rceil \quad (81)$$

where $0 < \alpha \leq 1$, then the capacity pre-log is *at most* $(1 + \alpha)/2$ which implies that $L \propto \sqrt{\text{SNR}}$ is optimal for achieving a pre-log of 3/4. We remark that the best known oversampling factor to achieve a pre-log of 3/4 for the model (19) is $L \propto \sqrt{\text{SNR}}$. We also remark that the upper bound derived in [38] was subsequently specialized to the additive-noise-free case in [39] (cf. (141)-(143)).

5) We briefly discuss sufficient statistics for the continuous-time phase noise channel. One expects intuitively at any SNR that

$$\lim_{L \rightarrow \infty} I(X^b; Y^{bL}) = I(x(t); r(t)). \quad (82)$$

This is because at infinite sampling rate, one captures essentially the entire received waveform. In general, it seems that an

infinite number of projections per symbol are needed to obtain sufficient statistics for all SNRs. For example, consider the Karhunen-Loève expansion of $U(t) = e^{j\Theta(t)}$ on $t \in [0, T_s]$, for which we have²

$$U(t) \stackrel{\text{m.s.}}{=} \sum_{i=0}^{\infty} U_i f_i(t) \quad (83)$$

where $\{f_i(t)\}$ are the orthonormal functions [40, Sec. 6.1]:

$$f_i(t) = \sqrt{\frac{2}{T_s + \lambda_i}} \begin{cases} \cos(\alpha_i(t - T_s/2)), & i \text{ odd} \\ \sin(\alpha_i(t - T_s/2)), & i \text{ even} \end{cases} \quad (84)$$

where α_i is the solution to

$$2 \arctan(\alpha_i/(\beta\pi)) + \alpha_i T_s = i\pi, \quad i = 0, 1, \dots \quad (85)$$

and the $\{U_i\}$ are uncorrelated random variables with variance λ_i where

$$\lambda_i = \frac{2\pi\beta}{\pi^2\beta^2 + \alpha_i^2}. \quad (86)$$

Suppose that one symbol X is transmitted and consider a rectangular pulse for simplicity. We have

$$r(t) = X e^{j\Theta(t)} + n(t) = \sum_{i=0}^{\infty} XU_i f_i(t) + n(t). \quad (87)$$

We conclude, in this simplified case, that

$$I(X; \{\Gamma_i\}_{i=0}^{\infty}) = I(x(t); r(t)) \quad (88)$$

where

$$\Gamma_i = \int_0^{T_s} r(t) f_i^*(t) dt, \quad i = 0, 1, \dots \quad (89)$$

i.e., $\{\Gamma_i\}_{i=0}^{\infty}$ are sufficient statistics for X . Therefore, an infinite number of projections per symbol seems to be needed to have sufficient statistics in general. Moreover, we believe that a finite subset of $\{\Gamma_i\}_{i=0}^{\infty}$ captures essentially all the information in the received waveform at a given SNR, and that larger subsets would be needed at larger SNRs. The discrete-time model based on the multi-sample receiver in Fig. 3 seems to be easier to analyze than the discrete-time model (89).

6) Minimum energy per information bit is an important metric at low SNR. For example, Fig. 12 plots the information rates of Fig. 8 against E_b/N_0 , where the energy per information bit is $E_b = P/R$ and R is the information rate in bits/symbol. We notice a significant impact on the minimum E_b due to phase noise. Furthermore, oversampling does not affect the rate at low E_b/N_0 , which suggests that using symbol-rate sampling suffices and that several results available in the literature on noncoherent fading channels and discrete-time phase noise channels (with the commonly-used approximation) should remain valid, e.g., see Fig. 2–Fig. 5 in [14].

² We use $\stackrel{\text{m.s.}}{=}$ to indicate convergence in mean-square sense.

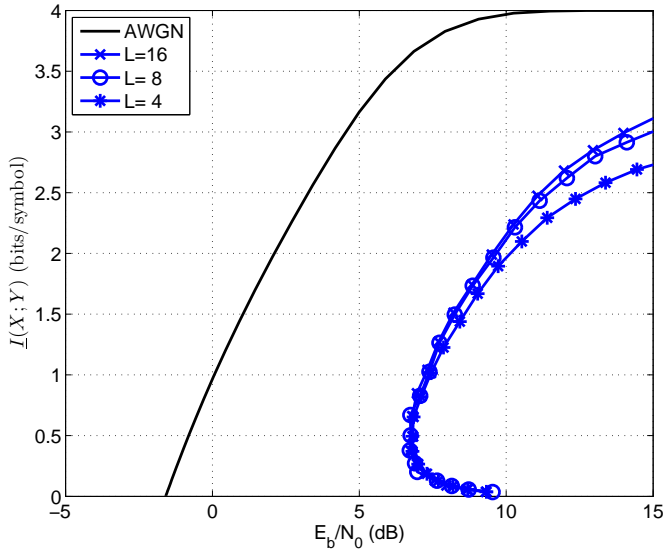


Fig. 12. Rates vs E_b/N_0 for 16-QAM, square transmit-pulse and multi-sample receiver at $f_{\text{HWHM}}T_s = 0.125$.

VIII. CONCLUSION

We studied a waveform channel impaired by Wiener phase noise and AWGN. A discrete-time channel model based on oversampling was derived taking into account filtering effects on phase noise. At high SNR, the multi-sample receiver achieves rates that grow logarithmically with SNR with at least a 1/2 pre-log factor, if the number of samples per symbol grows with the cubic root of the SNR. In addition, we computed via numerical simulations lower bounds on the information rates achieved by the multi-sample receiver. We observed that the required oversampling rate depends on the linewidth of the phase noise, the shape of the transmit-pulse and the SNR. The results demonstrate that multi-sample receivers increase the information rate for both strong and weak phase noise at high SNR. We compared our results with the results obtained by using other discrete-time models. Finally, we showed for an approximate discrete-time model of the multi-sample receiver that phase modulation achieves a pre-log of at least 1/4 while amplitude modulation achieves a pre-log of 1/2, if the number of samples per symbol grows with the square root of the SNR. Thus, we demonstrated that the overall capacity pre-log is 3/4 which is greater than the capacity pre-log of the (approximate) discrete-time Wiener phase noise channel with only one sample per symbol. The impact of oversampling on the capacity of non-Wiener phase noise channels, or multi-input multi-output (MIMO) phase noise channels, are open problems.

ACKNOWLEDGEMENT

We thank the reviewers and the Associate Editor for useful comments.

APPENDIX A AMPLITUDE MODULATION

This Appendix provides a proof of Theorem 1. We set $T_s = 1$ for simplicity. Since X_A^b is i.i.d., we have

$$\begin{aligned}
 I(X_A^b; \mathbf{Y}^b) &\stackrel{(a)}{=} \sum_{k=1}^b I(X_{A,k}; \mathbf{Y}^b | X_A^{k-1}) \\
 &\stackrel{(b)}{=} \sum_{k=1}^b \mathbf{H}(X_{A,k}) - \mathbf{H}(X_{A,k} | \mathbf{Y}^b, X_A^{k-1}) \\
 &\stackrel{(c)}{\geq} \sum_{k=1}^b I(X_{A,k}; \mathbf{Y}_k) \\
 &\stackrel{(d)}{\geq} \sum_{k=1}^b I(X_{A,k}; V_k)
 \end{aligned} \tag{90}$$

where

$$V_k = \sum_{\ell=1}^L |Y_{(k-1)L+\ell}|^2. \tag{91}$$

Step (a) follows from the chain rule of mutual information, (b) follows from the independence of $X_{A,1}, X_{A,2}, \dots, X_{A,b}$, (c) holds because conditioning does not increase entropy, and (d) follows from the data processing inequality. Since X_A^b is identically distributed, we find that V^b is also identically distributed and we have, for $k \geq 2$,

$$I(X_{A,k}; V_k) = I(X_{A,1}; V_1). \tag{92}$$

In the rest of this section, we consider only one symbol ($k = 1$) and drop the time index. By combining (91) and (19), we have

$$\begin{aligned}
 V &= \sum_{\ell=1}^L (X_A^2 \Delta^2 |F_\ell|^2 + 2X_A \Delta \Re[e^{j\Phi x} e^{j\Theta_\ell} F_\ell N_\ell^*] + |N_\ell|^2) \\
 &= X_A^2 \Delta G + 2X_A \Delta Z_1 + Z_0
 \end{aligned} \tag{93}$$

where G , Z_1 and Z_0 are defined as

$$G \equiv \frac{1}{L} \sum_{\ell=1}^L |F_\ell|^2 \tag{94}$$

$$Z_1 \equiv \sum_{\ell=1}^L \Re[e^{j\Phi x} e^{j\Theta_\ell} F_\ell N_\ell^*] \tag{95}$$

$$Z_0 \equiv \sum_{\ell=1}^L |N_\ell|^2. \tag{96}$$

The second-order statistics of Z_1 and Z_0 are

$$\begin{aligned}
 \mathbb{E}[Z_1] &= 0 & \text{Var}[Z_1] &= \mathbb{E}[G] \sigma_N^2 / 2 \\
 \mathbb{E}[Z_0] &= \sigma_N^2 & \text{Var}[Z_0] &= \sigma_N^4 \Delta \\
 \mathbb{E}[Z_1(Z_0 - \mathbb{E}[Z_0])] &= 0.
 \end{aligned} \tag{97}$$

By using the auxiliary-channel lower bound (cf. (39)), we have

$$I(X_A; V) \geq \mathbb{E}[-\log q_V(V)] - \mathbb{E}[-\log q_{V|X_A}(V|X_A)] \tag{98}$$

where $q_{V|X_A}(v|x_A)$ is the conditional distribution of the auxiliary channel, which we choose to be

$$q_{V|X_A}(v|x_A) = \frac{1}{\sqrt{4\pi x_A^2 \Delta^2 \sigma_N^2}} \exp\left(-\frac{(v - x_A^2 \Delta \tilde{G} - \sigma_N^2)^2}{4x_A^2 \Delta^2 \sigma_N^2}\right) \quad (99)$$

with $0 < \tilde{G} \leq 1$ and

$$q_V(v) = \int_0^\infty p_{X_A}(x_A) q_{V|X_A}(v|x_A) dx_A \quad (100)$$

where $p_{X_A}(\cdot)$ is the (true) pdf of X_A . The intuition behind the choice of (99) is given in Remark 3 below. It follows that

$$\begin{aligned} \mathbb{E}[-\log(q_{V|X_A}(V|X_A))] &= \mathbb{E}\left[\frac{(V - X_A^2 \Delta \tilde{G} - \sigma_N^2)^2}{4X_A^2 \Delta^2 \sigma_N^2}\right] \\ &+ \log \Delta + \frac{1}{2} \log(4\pi \sigma_N^2) + \frac{1}{2} \mathbb{E}[\log(X_A^2)] \end{aligned} \quad (101)$$

and by using (93) and (97), we have

$$\begin{aligned} \mathbb{E}\left[\frac{(V - X_A^2 \Delta \tilde{G} - \sigma_N^2)^2}{4X_A^2 \Delta^2 \sigma_N^2}\right] &= \frac{1}{4\sigma_N^2} \mathbb{E}[X_A^2] \mathbb{E}[(G - \tilde{G})^2] + \frac{1}{\sigma_N^2} \mathbb{E}[Z_1^2] \\ &+ \frac{1}{4\Delta^2 \sigma_N^2} \mathbb{E}\left[\frac{1}{X_A^2}\right] \mathbb{E}[(Z_0 - \sigma_N^2)^2] + \frac{1}{\sigma_N^2} \mathbb{E}[X_A] \mathbb{E}[(G - \tilde{G})Z_1] \\ &+ \frac{1}{2\Delta \sigma_N^2} \mathbb{E}[G - 1] \mathbb{E}[Z_0 - \sigma_N^2] + \frac{1}{\Delta \sigma_N^2} \mathbb{E}\left[\frac{1}{X_A}\right] \mathbb{E}[Z_1(Z_0 - \sigma_N^2)] \\ &= \frac{1}{4\sigma_N^2} P \mathbb{E}[(G - \tilde{G})^2] + \frac{1}{2} \mathbb{E}[G] + \frac{\sigma_N^2}{4\Delta} \mathbb{E}\left[\frac{1}{X_A^2}\right] \end{aligned} \quad (102)$$

where we also used

$$\mathbb{E}[(G - \tilde{G})Z_1] = 0. \quad (103)$$

Substituting (102) into (101) and using $\mathbb{E}[G] \leq 1$ yield

$$\begin{aligned} \mathbb{E}[-\log(q_{V|X_A}(V|X_A))] &\leq \log \Delta + \frac{1}{2} \log(4\pi \sigma_N^2) + \frac{1}{2} \mathbb{E}[\log(X_A^2)] \\ &+ \frac{P}{4\sigma_N^2} \mathbb{E}[(G - \tilde{G})^2] + \frac{1}{2} + \frac{\sigma_N^2}{4\Delta} \mathbb{E}\left[\frac{1}{X_A^2}\right]. \end{aligned} \quad (104)$$

It is convenient to define $X_P \equiv X_A^2$. The input distribution of X_P is

$$p_{X_P}(x_P) = \begin{cases} \frac{1}{\lambda} \exp\left(-\frac{x_P - \lambda}{\lambda}\right), & x_P \geq \lambda \\ 0, & \text{otherwise} \end{cases} \quad (105)$$

where $\lambda = P/2$. It follows from (100) and (105) that

$$\begin{aligned} q_V(v) &= \int_\lambda^\infty \frac{1}{\lambda} \exp\left(-\frac{x_P - \lambda}{\lambda}\right) q_{V|X_P}(v|x_P) dx_P \\ &\leq e f_V(v) \end{aligned} \quad (106)$$

where

$$q_{V|X_P}(v|x_P) = q_{V|X_A}(v|\sqrt{x_P}) \quad (107)$$

and

$$f_V(v) \equiv \int_0^\infty \frac{1}{\lambda} \exp\left(-\frac{x_P}{\lambda}\right) q_{V|X_P}(v|x_P) dx_P. \quad (108)$$

The inequality (106) follows from the non-negativity of the integrand. By combining (99), (107), (108) and making the change of variables $x = x_P \Delta$, we have

$$\begin{aligned} f_V(v) &= \int_0^\infty \frac{e^{-x/(\lambda\Delta)}}{\lambda\Delta} \frac{1}{\sqrt{4\pi x \Delta \sigma_N^2}} \exp\left(-\frac{(v - x - \sigma_N^2)^2}{4x \Delta \sigma_N^2}\right) dx \\ &= \frac{1}{\sqrt{\lambda\Delta(\lambda\Delta + 4\Delta\sigma_N^2)}} \times \\ &\exp\left(\frac{2}{4\Delta\sigma_N^2} \left[v - \sigma_N^2 - |v - \sigma_N^2| \sqrt{1 + \frac{4\Delta\sigma_N^2}{\lambda\Delta}} \right]\right) \end{aligned} \quad (109)$$

where we used equation (140) in Appendix A of [41]:

$$\begin{aligned} \int_0^\infty \frac{1}{a} \exp\left(-\frac{x}{a}\right) \frac{1}{\sqrt{\pi b x}} \exp\left(-\frac{(u-x)^2}{bx}\right) dx \\ = \frac{1}{\sqrt{a(a+b)}} \exp\left(\frac{2}{b} \left[u - |u| \sqrt{1 + \frac{b}{a}} \right]\right). \end{aligned} \quad (110)$$

Therefore, we have

$$\begin{aligned} \mathbb{E}[-\log(f_V(V))] &= \frac{1}{2} \log(\Delta^2(\lambda^2 + 4\lambda\sigma_N^2)) \\ &- \frac{1}{2\Delta\sigma_N^2} \left[\mathbb{E}[V - \sigma_N^2] - \mathbb{E}[|V - \sigma_N^2|] \sqrt{1 + \frac{4\sigma_N^2}{\lambda}} \right] \\ &\stackrel{(a)}{\geq} \log(\Delta\lambda) + \frac{1}{2\sigma_N^2\Delta} \mathbb{E}[V - \sigma_N^2] \left[\sqrt{1 + \frac{4\sigma_N^2}{\lambda}} - 1 \right] \\ &\stackrel{(b)}{\geq} \log(\Delta\lambda) \end{aligned} \quad (111)$$

where (a) holds because the logarithmic function is monotonic and $\mathbb{E}[|\cdot|] \geq \mathbb{E}[\cdot]$, and (b) holds because

$$\begin{aligned} \mathbb{E}[V - \sigma_N^2] &= \mathbb{E}[X_A^2] \Delta \mathbb{E}[G] + 2\mathbb{E}[X_A] \Delta \mathbb{E}[Z_1] + \mathbb{E}[Z_0] - \sigma_N^2 \\ &= P \Delta \mathbb{E}[G] \geq 0. \end{aligned} \quad (112)$$

The monotonicity of the logarithmic function and (106) yield

$$\begin{aligned} \mathbb{E}[-\log(q_V(V))] &\geq \mathbb{E}[-\log(e f_V(V))] \\ &\geq \log \Delta + \log \lambda - 1 \end{aligned} \quad (113)$$

where the last inequality follows from (111). It follows from (98), (104) and (113) that

$$\begin{aligned} I(X_A; V) &\geq \log \lambda - 1 - \frac{1}{2} \log(4\pi \sigma_N^2) - \frac{1}{2} \mathbb{E}[\log(X_A^2)] \\ &- \frac{P}{4\sigma_N^2} \mathbb{E}[(G - \tilde{G})^2] - \frac{1}{2} - \frac{\sigma_N^2}{4\Delta} \mathbb{E}\left[\frac{1}{X_A^2}\right]. \end{aligned} \quad (114)$$

We have

$$\mathbb{E}\left[\frac{1}{X_P}\right] \leq \frac{2}{P} \quad (115)$$

and

$$\begin{aligned} \mathbb{E} [\log (X_P)] &= \int_{\lambda}^{\infty} \frac{1}{\lambda} e^{-(x-\lambda)/\lambda} \log(x) dx \\ &\stackrel{(a)}{=} \log \lambda + \int_1^{\infty} e^{-(u-1)} \log(u) du \\ &\stackrel{(b)}{\leq} \log \lambda + 1 \end{aligned} \quad (116)$$

where (a) follows by the change of variables $u = x/\lambda$, and (b) holds because $\log(u) \leq u - 1$ for all $u > 0$. Substituting into (114), we obtain

$$\begin{aligned} I(X_A; V) - \frac{1}{2} \log \text{SNR} &\geq -2 - \frac{1}{2} \log(8\pi) - \frac{1}{2\text{SNR}\Delta} \\ &\quad - \frac{1}{4} \text{SNR} \mathbb{E} \left[(G - \tilde{G})^2 \right]. \end{aligned} \quad (117)$$

By combining (36), (90), (92) and (117), we have

$$\begin{aligned} I(X_A; Y) - \frac{1}{2} \log \text{SNR} &\geq -2 - \frac{1}{2} \log(8\pi) - \frac{1}{2\text{SNR}\Delta} \\ &\quad - \frac{1}{4} \text{SNR} \mathbb{E} \left[(G - \tilde{G})^2 \right]. \end{aligned} \quad (118)$$

Since (118) is valid for any $\tilde{G} \in (0, 1]$, we choose \tilde{G} to maximize the right hand side of (118). The optimal \tilde{G} is

$$\arg \min_{\tilde{G}} \mathbb{E} \left[(G - \tilde{G})^2 \right] = \mathbb{E}[G]. \quad (119)$$

Since $L = \lceil \sqrt[3]{\beta^2 \text{SNR}} \rceil$ and $\Delta = 1/L$, it follows that

$$\lim_{\text{SNR} \rightarrow \infty} \text{SNR}\Delta = \infty \quad \text{and} \quad \lim_{\text{SNR} \rightarrow \infty} \text{SNR}\Delta^3 = \frac{1}{\beta^2}. \quad (120)$$

Moreover, we have (see Appendix C)

$$\begin{aligned} \lim_{\text{SNR} \rightarrow \infty} \text{SNR} \text{Var}(G) &= \lim_{\text{SNR} \rightarrow \infty} \text{SNR}\Delta^3 \cdot \lim_{\Delta \rightarrow 0} \frac{\text{Var}(G)}{\Delta^3} \\ &= \frac{1}{\beta^2} \cdot \frac{4(\pi\beta)^2}{45} = \frac{4\pi^2}{45}. \end{aligned} \quad (121)$$

Hence, for $\tilde{G} = \mathbb{E}[G]$, we have

$$\lim_{\text{SNR} \rightarrow \infty} I(X_A; Y) - \frac{1}{2} \log \text{SNR} \geq -2 - \frac{1}{2} \log(8\pi) - \frac{\pi^2}{45}. \quad (122)$$

Remark 3: We motivate the auxiliary channel in (99). We first express the auxiliary channel as \tilde{V} :

$$\tilde{V} = X_A^2 \Delta \tilde{G} + 2X_A \Delta \tilde{Z}_1 + \tilde{Z}_0 \quad (123)$$

where \tilde{G} , \tilde{Z}_1 and \tilde{Z}_0 are defined as

$$\tilde{G} \equiv \mathbb{E}[G] \quad (124)$$

$$\tilde{Z}_1 \equiv \sum_{\ell=1}^L \Re[e^{j\Phi_X} e^{j\Theta_\ell} N_\ell^*] \quad (125)$$

$$\tilde{Z}_0 \equiv \sigma_N^2. \quad (126)$$

We make this choice for \tilde{V} because Z_1 and Z_0 converge (in mean square) to \tilde{Z}_1 and \tilde{Z}_0 , respectively, as $L \rightarrow \infty$. Moreover, \tilde{Z}_1 is Gaussian and \tilde{Z}_0 is a constant, which are easier quantities to handle than Z_1 and Z_0 .

APPENDIX B PHASE MODULATION

This Appendix provides a proof of Theorem 2. We assume that $T_s = 1$ and $\sigma_N^2 = 1$ for simplicity. By using the chain rule, we have

$$\begin{aligned} I(\Phi_X^n; \Psi^n | X_A^n) &= \sum_{k=1}^n I(\Phi_{X,k}; \Psi^n | X_A^n, \Phi_X^{k-1}) \\ &\stackrel{(a)}{\geq} \sum_{k=2}^n I(\Phi_{X,k}; \Psi^n | X_A^n, \Phi_X^{k-1}) \\ &\stackrel{(b)}{\geq} \sum_{k=2}^n I(\Phi_{X,k}; \tilde{\Psi}_k | X_A^n, \Phi_X^{k-1}) \end{aligned} \quad (127)$$

where $\tilde{\Psi}_k$ is a deterministic function of $(\Psi^n, X_A^n, \Phi_X^{k-1})$. Inequality (a) follows from the non-negativity of mutual information and (b) follows from the data processing inequality. We choose

$$\tilde{\Psi}_k = \frac{\Psi_{(k-1)L+1}}{\sqrt{\Delta}} \left(\frac{\Psi_{(k-1)L}}{X_{k-1}\Delta} \right)^*. \quad (128)$$

The intuition behind the choice of (128) is outlined in Remark 4 below. We express $\tilde{\Psi}_k$ as

$$\tilde{\Psi}_k = \left(|X_k| \sqrt{\Delta} e^{j\Phi_{X,k}} + \tilde{N}_k \right) \left(1 + \tilde{Z}_{k-1} \right) e^{jW_{(k-1)L+1}} \quad (129)$$

where

$$\tilde{Z}_k \equiv \frac{N_{kL}^* e^{-j\Theta_{kL}}}{X_k^* \Delta} \quad (130)$$

and

$$\tilde{N}_k \equiv \frac{N_{(k-1)L+1} e^{-j\Theta_{(k-1)L+1}}}{\sqrt{\Delta}}. \quad (131)$$

The processes \tilde{N}_k and \tilde{Z}_{k-1} are statistically independent and

$$\tilde{N}_k \sim \mathcal{N}_{\mathbb{C}}(0, 1) \quad (132)$$

$$\tilde{Z}_{k-1} \left\{ |X_{k-1}| = |x_{k-1}| \right\} \sim \mathcal{N}_{\mathbb{C}} \left(0, \frac{1}{|x_{k-1}|^2 \Delta} \right). \quad (133)$$

The notation (133) means that, conditioned on $\{|X_{k-1}| = |x_{k-1}|\}$, \tilde{Z}_{k-1} is a Gaussian random variable with mean 0 and variance $1/(|x_{k-1}|^2 \Delta)$. Moreover, $W_{(k-1)L+1}$ is statistically independent of \tilde{N}_k and \tilde{Z}_{k-1} . The choice of $\tilde{\Psi}_k$ in (128) implies that

$$I(\Phi_{X,k}; \tilde{\Psi}_k | X_A^n, X^{k-1}) = I(\Phi_{X,k}; \tilde{\Psi}_k | X_{A,k}, X_{k-1}). \quad (134)$$

Define $\tilde{\Phi}_{\Psi,k} \equiv \arg(\tilde{\Psi}_k)$ and

$$q_{\tilde{\Phi}_{\Psi,k} | \Phi_X}(\phi_y | \phi_x) \equiv \frac{\exp(\alpha \cos(\phi_y - \phi_x))}{2\pi I_0(\alpha)} \quad (135)$$

where $I_0(\cdot)$ is the zeroth-order modified Bessel function of the first kind and $\alpha > 0$. This distribution is known as Tikhonov (or von Mises) distribution [42]. Furthermore, define

$$\begin{aligned} q_{\tilde{\Phi}_{\Psi,k} | X_A, X_{k-1}}(\phi_y || x_k, x_{k-1}) & \\ &\equiv \int_{-\pi}^{\pi} p_{\Phi_{X,k} | X_A, X_{k-1}}(\phi_x || x_k, x_{k-1}) q_{\tilde{\Phi}_{\Psi,k} | \Phi_X}(\phi_y | \phi_x) d\phi_x \\ &= \frac{1}{2\pi}. \end{aligned} \quad (136)$$

The last equality holds because X_1, \dots, X_n are statistically independent and $\Phi_{X,k}$ is independent of $X_{A,k}$ with a uniform distribution on $[-\pi, \pi)$. We have

$$\begin{aligned}
 & I(\Phi_{X,k}; \tilde{\Psi}_k | X_{A,k}, X_{k-1}) \\
 & \stackrel{(a)}{\geq} I(\Phi_{X,k}; \tilde{\Phi}_{\Psi,k} | X_{A,k}, X_{k-1}) \\
 & \stackrel{(b)}{\geq} \mathbb{E} \left[\log q_{\tilde{\Phi}_{\Psi,k} | \Phi_{X,k}}(\tilde{\Phi}_{\Psi,k} | \Phi_{X,k}) \right] \\
 & - \mathbb{E} \left[\log q_{\tilde{\Phi}_{\Psi,k} | X_{A,k}, X_{k-1}}(\tilde{\Phi}_{\Psi,k} | |X_k|, X_{k-1}) \right] \\
 & \stackrel{(c)}{=} \log(2\pi) - \log(2\pi I_0(\alpha)) + \alpha \mathbb{E} \left[\cos(\tilde{\Phi}_{\Psi,k} - \Phi_{X,k}) \right] \\
 & = -\log(I_0(\alpha)) + \alpha \mathbb{E} \left[\cos(\tilde{\Phi}_{\Psi,k} - \Phi_{X,k}) \right] \\
 & \stackrel{(d)}{\geq} \frac{1}{2} \log \alpha - \alpha + \alpha \mathbb{E} \left[\cos(\tilde{\Phi}_{\Psi,k} - \Phi_{X,k}) \right] \\
 & \geq \frac{1}{2} \log \alpha - \alpha \frac{\sigma_W^2}{2} - \frac{4\alpha}{\text{SNR}\Delta} \tag{137}
 \end{aligned}$$

where (a) follows from the data processing inequality, (b) follows by extending the result of the auxiliary-channel lower bound (cf. (39)), (c) follows from (135) and (136), (d) follows from [43, Lemma 2]

$$I_0(z) \leq \frac{\sqrt{\pi}}{2} \frac{e^z}{\sqrt{z}} \leq \frac{e^z}{\sqrt{z}} \tag{138}$$

and the last inequality holds because

$$\mathbb{E} \left[\cos(\tilde{\Phi}_{\Psi,k} - \Phi_{X,k}) \right] \geq 1 - \frac{\sigma_W^2}{2} - \frac{4}{\text{SNR}\Delta} \tag{139}$$

for $\text{SNR}\Delta > 2$, as we will show. Define

$$S_k \equiv 1 + \tilde{Z}_k \tag{140}$$

$$\hat{\Psi}_k \equiv |X_k| \sqrt{\Delta} e^{j\Phi_{X,k}} + \tilde{N}_k. \tag{141}$$

Therefore, we have

$$\begin{aligned}
 & \mathbb{E} \left[\cos(\tilde{\Phi}_{\Psi,k} - \Phi_{X,k}) \right] \\
 & \stackrel{(a)}{=} \mathbb{E} \left[\cos(W_{(k-1)L+1} + \Phi_{S,k-1} + \hat{\Phi}_{\Psi,k} - \Phi_{X,k}) \right] \\
 & \stackrel{(b)}{=} \mathbb{E} \left[\cos(W_{(k-1)L+1} + \Phi_{S,k-1}) \right] \mathbb{E} \left[\cos(\hat{\Phi}_{\Psi,k} - \Phi_{X,k}) \right] \\
 & - \mathbb{E} \left[\sin(W_{(k-1)L+1} + \Phi_{S,k-1}) \right] \mathbb{E} \left[\sin(\hat{\Phi}_{\Psi,k} - \Phi_{X,k}) \right] \tag{142}
 \end{aligned}$$

where $\Phi_{S,k} \equiv \arg(S_k)$ and $\hat{\Phi}_{\Psi,k} \equiv \arg(\hat{\Psi}_k)$. Step (a) follows from (129) while step (b) follows from the trigonometric relation $\cos(A+B) = \cos(A)\cos(B) - \sin(A)\sin(B)$ and because $W_{(k-1)L+1} + \Phi_{S,k-1}$ is independent of $\hat{\Phi}_{\Psi,k}$ and $\Phi_{X,k}$.

By using Lemma 6 in Appendix D, we have

$$\mathbb{E} \left[\cos(\hat{\Phi}_{\Psi,k} - \Phi_{X,k}) \middle| X_{A,k} = |x_k| \right] \geq 1 - \frac{1}{|x_k|^2 \Delta} \tag{143}$$

$$\mathbb{E} \left[\sin(\hat{\Phi}_{\Psi,k} - \Phi_{X,k}) \middle| X_{A,k} = |x_k| \right] = 0. \tag{144}$$

Equations (142) and (144) imply that we do not need to compute $\mathbb{E} \left[\sin(W_{(k-1)L+1} + \Phi_{S,k-1}) \right]$. We have

$$\begin{aligned}
 & \mathbb{E} \left[\cos(W_{(k-1)L+1} + \Phi_{S,k-1}) \right] \\
 & = \mathbb{E} \left[\cos(W_{(k-1)L+1}) \right] \mathbb{E} \left[\cos(\Phi_{S,k-1}) \right] \\
 & - \mathbb{E} \left[\sin(W_{(k-1)L+1}) \right] \mathbb{E} \left[\sin(\Phi_{S,k-1}) \right] \tag{145}
 \end{aligned}$$

because $W_{(k-1)L+1}$ and $\Phi_{S,k-1}$ are independent. Since $W_{(k-1)L+1}$ is Gaussian with mean 0 and variance $\sigma_W^2 = 2\pi\beta\Delta$, the characteristic function of $W_{(k-1)L+1}$ is

$$\mathbb{E} \left[e^{jW_{(k-1)L+1}} \right] = e^{-\sigma_W^2/2} \tag{146}$$

and by using the linearity of expectation, we have

$$\mathbb{E} \left[\cos(W_{(k-1)L+1}) \right] = \Re \left[\mathbb{E} \left[e^{jW_{(k-1)L+1}} \right] \right] = e^{-\sigma_W^2/2} \tag{147}$$

$$\mathbb{E} \left[\sin(W_{(k-1)L+1}) \right] = \Im \left[\mathbb{E} \left[e^{jW_{(k-1)L+1}} \right] \right] = 0 \tag{148}$$

where $\Re[\cdot]$ and $\Im[\cdot]$ denote the real and imaginary parts, respectively. By using Lemma 6 in Appendix D again, we have

$$\mathbb{E} \left[\cos(\Phi_{S,k-1}) \middle| X_{k-1} = x_{k-1} \right] \geq 1 - \frac{1}{|x_{k-1}|^2 \Delta}. \tag{149}$$

It follows from (145), (147), (148) and (149) that

$$\begin{aligned}
 & \mathbb{E} \left[\cos(W_{(k-1)L+1} + \Phi_{S,k-1}) \right] \\
 & \geq e^{-\sigma_W^2/2} \left(1 - \mathbb{E} \left[\frac{1}{|X_{k-1}|^2} \right] \frac{1}{\Delta} \right). \tag{150}
 \end{aligned}$$

By combining (142), (143), (144) (150), we have (for $P\Delta > 2$)

$$\begin{aligned}
 & \mathbb{E} \left[\cos(\tilde{\Phi}_{\Psi,k} - \Phi_{X,k}) \right] \\
 & \geq e^{-\sigma_W^2/2} \left(1 - \mathbb{E} \left[\frac{1}{|X_{k-1}|^2} \right] \frac{1}{\Delta} \right) \left(1 - \mathbb{E} \left[\frac{1}{|X_k|^2} \right] \frac{1}{\Delta} \right) \\
 & \stackrel{(a)}{\geq} e^{-\sigma_W^2/2} \left(1 - \frac{2}{P\Delta} \right)^2 \\
 & \stackrel{(b)}{\geq} e^{-\sigma_W^2/2} - \frac{4}{P\Delta} \\
 & \stackrel{(c)}{\geq} 1 - \frac{\sigma_W^2}{2} - \frac{4}{P\Delta} \tag{151}
 \end{aligned}$$

where (a) holds because $|X_k|^2 \geq P/2$ and $|X_{k-1}|^2 \geq P/2$, while (b) follows from $e^{-\sigma_W^2/2} \leq 1$ and the non-negativity of $4/(P\Delta)^2$ and (c) follows from $e^{-x} \geq 1 - x$.

It follows from (127), (134) and (137) that

$$\frac{1}{b} I(\Phi_X^b; \Psi^b | X_A^b) \geq \frac{b-1}{b} \left[\frac{1}{2} \log \alpha - \alpha\pi\beta\Delta - \frac{4\alpha}{\text{SNR}\Delta} \right]. \tag{152}$$

Hence, we have

$$\begin{aligned}
 I(\Phi_X; \Psi | X_A) & = \lim_{b \rightarrow \infty} \frac{1}{b} I(\Phi_X^b; \Psi^b | X_A^b) \\
 & \geq \frac{1}{2} \log \alpha - \alpha\pi\beta\Delta - \frac{4\alpha}{\text{SNR}\Delta}. \tag{153}
 \end{aligned}$$

Since the lower bound (153) is valid for any $\alpha > 0$, we have

$$\begin{aligned} I(\Phi_X; \Psi|X_A) &\geq \max_{\alpha>0} \frac{1}{2} \log \alpha - \alpha \left(\pi\beta\Delta + \frac{4}{\text{SNR}\Delta} \right) \\ &= -\frac{1}{2} \log \left(2\pi\beta\Delta + \frac{8}{\text{SNR}\Delta} \right) - \frac{1}{2} \\ &= -\frac{1}{2} \log \left(\frac{2\pi\beta}{L} + \frac{8L}{\text{SNR}} \right) - \frac{1}{2} \end{aligned} \quad (154)$$

where we used $\Delta = 1/L$ in the last equation. We maximize the lower bound (154) over L to obtain ³

$$L = \sqrt{\pi\beta\text{SNR}}/2. \quad (155)$$

By choosing an oversampling factor $L = \lceil \sqrt{\pi\beta\text{SNR}}/2 \rceil$, it follows that

$$\lim_{\text{SNR} \rightarrow \infty} I(\Phi_X; \Psi|X_A) - \frac{1}{4} \log \text{SNR} \geq -\frac{1}{4} \log(64\pi\beta) - \frac{1}{2}. \quad (156)$$

The proof of (43) is similar to the proof in Appendix A for the full model and is omitted.⁴

Remark 4: We outline the intuition for choosing $\tilde{\Psi}_k$ in (128). The basic idea is to process $(\Psi^n, X_A^n, \Phi_X^{k-1})$ in three steps: first estimate the phase noise, then cancel it, then decode. We outline the motivation for each step:

1) Since the past inputs X^{k-1} and outputs \mathbf{Y}^{k-1} are available, one may use the simple estimator

$$e^{j\hat{\Theta}_{k'}} \equiv \frac{\Psi_{k'}}{X_{\lceil k'/L \rceil} \Delta} \quad (157)$$

to estimate $\Theta_{k'}$ for $k' = 1, \dots, (k-1)L$. This is a reasonable estimate as long as the energy per sample is large relative to the noise variance per sample, i.e., when $\text{SNR}\Delta \gg 1$.

2) Next, we use the previous estimates to cancel from \mathbf{Y}_k^n the phase noise that accumulated up to sample $(k-1)L$. More precisely, we use only the most recent estimate $\hat{\Theta}_{(k-1)L}$. We make this choice because the discrete-time Wiener process $\{\Theta_k\}$ is a first-order Markov process so, conditioned on Θ_{kL} , the random variables $\Theta_{kL+1}, \dots, \Theta_{nL}$ are independent of $\Theta_0, \dots, \Theta_{kL-1}$. This means that if the SNR is high enough so that $\hat{\Theta}_{k'}$ is an accurate estimate of $\Theta_{k'}$ for $k' = 1, \dots, (k-1)L$, then it would suffice to use only $\hat{\Theta}_{(k-1)L}$.

3) Since the input is i.i.d. and there is no inter-symbol interference, we discard Ψ_{k+1}^n and use only Ψ_k (after canceling the phase noise) for decoding $\Phi_{X,k}$. Moreover, we use only the first sample $\Psi_{(k-1)L+1}$ in Ψ_k . This is because, in absence of additive noise, we have

$$\begin{aligned} I(\Phi_{X,k}; \Psi_k) &= I(\Phi_{X,k}; \{\Phi_{\Psi, (k-1)L+1} : 1 \leq \ell \leq L\}) \\ &= I(\Phi_{X,k}; \Phi_{\Psi, (k-1)L+1}, \{W_{(k-1)L+\ell} : 2 \leq \ell \leq L\}) \\ &= I(\Phi_{X,k}; \Phi_{\Psi, (k-1)L+1}) \\ &= I(\Phi_{X,k}; \Psi_{(k-1)L+1}). \end{aligned}$$

³Ignoring $L \in \mathbb{Z}$.

⁴The inequality (118) is valid for the approximate model except that G is set to 1 because $F_k = 1$ in the approximate model. Hence, by setting $\tilde{G} = 1$, the term $-\pi^2/45$ in (40) does not appear in (43).

APPENDIX C

SUPPORTING LEMMA FOR APPENDIX A

The following lemma is used in Appendix A.

Lemma 5: For G in (94) with $T_s = 1$, we have

$$\lim_{\Delta \rightarrow 0} \frac{\text{Var}(G)}{\Delta^3} = \frac{4}{45}(\pi\beta)^2. \quad (158)$$

Proof: Using the definition of G in (94), we have

$$\text{Var}(G) = \text{Var} \left(\frac{1}{L} \sum_{\ell=1}^L |F_\ell|^2 \right) = \frac{1}{L} \text{Var}(|F_1|^2) \quad (159)$$

because $\{F_k\}$ is an i.i.d. process. The independence follows because increments of a Wiener process over disjoint time intervals are independent and because functions of independent random variables are also independent. The identical distribution property follows from the rectangular pulse shape⁵ and that the integrations are over increments of a Wiener process with equal length. By using the formula in [44, Theorem 1] for computing moments of filtered Wiener phase noise (specifically $\mathbb{E}[|F_1|^{2k}]$ where k is a positive integer), we have

$$\mathbb{E}[|F_1|^2] = 2 \frac{a-1-\log a}{(\log a)^2} \quad (160)$$

and

$$\begin{aligned} \mathbb{E}[|F_1|^4] &= \frac{783 - 784a + a^4 + (540 + 240a) \log a + 144(\log a)^2}{18(\log a)^4}. \end{aligned} \quad (161)$$

where

$$a \equiv e^{-\pi\beta\Delta}. \quad (162)$$

It follows from (161) and (160) that

$$\begin{aligned} \text{Var}(|F_1|^2) &= \mathbb{E}[|F_1|^4] - (\mathbb{E}[|F_1|^2])^2 \\ &= \frac{711 - 640a - 72a^2 + a^4 + 12(33 + 32a) \log a + 72(\log a)^2}{18(\log a)^4} \end{aligned} \quad (163)$$

which implies that

$$\lim_{a \rightarrow 1} \frac{\text{Var}(|F_1|^2)}{(\log a)^2} = \frac{4}{45}. \quad (164)$$

Finally, (158) follows from (164), (162) and $L = 1/\Delta$ (because $T_s = 1$). \blacksquare

APPENDIX D

SUPPORTING LEMMAS FOR APPENDIX B

This appendix contains two lemmas. The main lemma is Lemma 6 which is used in Appendix B. Lemma 7 is a supporting lemma for Lemma 6.

⁵If the pulse is not rectangular, the process $\{F_k\}$ may not be identically distributed because the phase noise $e^{j\Theta(t)}$ is weighted in a given sample interval according to the pulse shape.

Lemma 6: Let R be a fixed positive real number and let $\Phi \equiv \arg(Y)$ where

$$Y = R + Z \quad (165)$$

and Z is a circularly-symmetric complex Gaussian random variable with mean 0 and variance 1. Then, we have

$$\mathbb{E}[\cos(\Phi)] \geq 1 - \frac{1}{R^2} \quad (166)$$

$$\mathbb{E}[\sin(\Phi)] = 0. \quad (167)$$

Proof: The probability density function of Φ is [45]

$$p_{\Phi}(\phi) = \frac{1}{2\pi} e^{-R^2} + \frac{1}{\sqrt{4\pi}} R \cos(\phi) e^{-R^2 \sin^2 \phi} \operatorname{erfc}(-R \cos \phi) \quad (168)$$

where $\operatorname{erfc}(\cdot)$ is the complementary error function

$$\operatorname{erfc}(z) \equiv \frac{2}{\sqrt{\pi}} \int_z^{\infty} e^{-t^2} dt. \quad (169)$$

Therefore, we have

$$\begin{aligned} \mathbb{E}[\cos(\Phi)] &\equiv \int_{-\pi}^{\pi} \cos(\phi) p_{\Phi}(\phi) d\phi \\ &\stackrel{(a)}{=} 2 \int_0^{\pi} \cos(\phi) p_{\Phi}(\phi) d\phi \\ &\stackrel{(b)}{=} \int_0^{\pi} \cos(\phi) \left[\frac{1}{\sqrt{\pi}} R \cos(\phi) e^{-R^2 \sin^2 \phi} \operatorname{erfc}(-R \cos \phi) \right] d\phi \\ &\stackrel{(c)}{\geq} \int_0^{\pi/2} \frac{R}{\sqrt{\pi}} \cos^2(\phi) e^{-R^2 \sin^2 \phi} \operatorname{erfc}(-R \cos \phi) d\phi \\ &\stackrel{(d)}{\geq} \int_0^{\pi/2} \frac{R}{\sqrt{\pi}} \cos^2(\phi) e^{-R^2 \sin^2 \phi} \left(2 - e^{-R^2 \cos^2 \phi} \right) d\phi \\ &= \int_0^{\pi/2} \frac{2R}{\sqrt{\pi}} \cos^2(\phi) e^{-R^2 \sin^2 \phi} d\phi - \frac{R}{\sqrt{\pi}} e^{-R^2} \int_0^{\pi/2} \cos^2 \phi d\phi \\ &\stackrel{(e)}{=} \int_0^{\pi/2} \frac{2R}{\sqrt{\pi}} \cos^2(\phi) e^{-R^2 \sin^2 \phi} d\phi - \frac{\sqrt{\pi}}{4} R e^{-R^2} \quad (170) \end{aligned}$$

where (a) follows because both $p_{\Phi}(\cdot)$ and $\cos(\phi)$ are even functions, (b) follows from (168) and $\int_0^{\pi} \cos \phi d\phi = 0$, (c) follows because the integrand is non-negative over the interval $\phi \in (\pi/2, \pi]$, (d) holds because $\operatorname{erfc}(-R \cos \phi) \geq 2 - e^{-R^2 \cos^2 \phi}$ (see Lemma 7) and $\cos^2(\phi) e^{-R^2 \sin^2 \phi} \geq 0$ and finally (e) follows by direct integration.

We bound the integral in (170) as follows

$$\begin{aligned} &\int_0^{\pi/2} \frac{2R}{\sqrt{\pi}} \cos^2 \phi e^{-R^2 \sin^2 \phi} d\phi \\ &\stackrel{(a)}{\geq} \frac{2R}{\sqrt{\pi}} \int_0^{\pi/2} (1 - \phi^2) e^{-R^2 \phi^2} d\phi \\ &= \frac{2R}{\sqrt{\pi}} \int_0^{\pi/2} e^{-R^2 \phi^2} d\phi - \frac{2R}{\sqrt{\pi}} \int_0^{\pi/2} \phi^2 e^{-R^2 \phi^2} d\phi \\ &\stackrel{(b)}{=} \operatorname{erf}\left(\frac{\pi}{2} R\right) - \frac{1}{2R^2} \operatorname{erf}\left(\frac{\pi}{2} R\right) + \frac{1}{2\sqrt{\pi} R} e^{-\pi^2 R^2/4} \\ &\stackrel{(c)}{\geq} \operatorname{erf}\left(\frac{\pi}{2} R\right) - \frac{1}{2R^2} \quad (171) \end{aligned}$$

where $\operatorname{erf}(\cdot)$ is the error function defined as

$$\operatorname{erf}(z) \equiv \frac{2}{\sqrt{\pi}} \int_0^z e^{-t^2} dt. \quad (172)$$

Step (a) follows from $\cos^2 \phi e^{-R^2 \sin^2 \phi} \geq (1 - \phi^2) e^{-R^2 \phi^2}$ (see Lemma 7), (b) follows by using the definition of $\operatorname{erf}(\cdot)$ and [46, 3.321(5)]:

$$\int_0^b t^2 e^{-a^2 t^2} dt = \frac{1}{2a^3} \left[\frac{\sqrt{\pi}}{2} \operatorname{erf}(ab) - ab e^{-a^2 b^2} \right] \quad (173)$$

and (c) holds because $\operatorname{erf}(\cdot) \leq 1$ and the last term is non-negative. Substituting back in (170) yields

$$\mathbb{E}[\cos(\Phi)] \geq \operatorname{erf}\left(\frac{\pi}{2} R\right) - \frac{1}{2R^2} - \frac{\sqrt{\pi}}{4} R e^{-R^2} \quad (174)$$

$$\geq 1 - e^{-\pi^2 R^2/4} - \frac{1}{2R^2} - \frac{\sqrt{\pi}}{4} R e^{-R^2} \quad (175)$$

where the last inequality follows from the relations $\operatorname{erf}(\pi R/2) = 1 - \operatorname{erfc}(\pi R/2)$ and $\operatorname{erfc}(\pi R/2) \leq e^{-\pi^2 R^2/4}$ (see [47, eq. (5)]). Therefore, we have

$$R^2 \mathbb{E}[\cos(\Phi)] \geq R^2 - \frac{4}{\pi^2 e} - \frac{1}{2} - \frac{\sqrt{\pi}}{4} \left(\frac{3}{2e} \right)^{3/2} \quad (176)$$

because

$$\max_x x^m e^{-ax^2} = \left(\frac{m}{2ae} \right)^{m/2} \quad (177)$$

for any $a > 0$ and positive integer m , which implies that $R^3 e^{-R^2} \leq (3/2e)^{3/2}$ and $R^2 e^{-\pi^2 R^2/4} \leq 4/\pi^2 e$. We conclude that

$$\mathbb{E}[\cos(\Phi)] \geq 1 - \frac{0.83}{R^2} \geq 1 - \frac{1}{R^2}. \quad (178)$$

Finally, we have

$$\mathbb{E}[\sin(\Phi)] \equiv \int_{-\pi}^{\pi} \sin(\phi) p_{\Phi}(\phi) d\phi = 0 \quad (179)$$

because the integrand is odd. ■

Lemma 7: The following bounds hold.

1) For $z \geq 0$:

$$\operatorname{erfc}(-z) \geq 2 - e^{-z^2}. \quad (180)$$

2) For $a \geq 0$ and $t \geq 0$:

$$\cos^2 t e^{-a \sin^2 t} \geq (1 - t^2) e^{-at^2}. \quad (181)$$

Proof:

1) Since for any real number z

$$\operatorname{erf}(-z) = -\operatorname{erf}(z) \quad (182)$$

$$\operatorname{erfc}(z) = 1 - \operatorname{erf}(z) \quad (183)$$

we have

$$\operatorname{erfc}(-z) = 1 - \operatorname{erf}(-z) = 1 + \operatorname{erf}(z) = 2 - \operatorname{erfc}(z). \quad (184)$$

To complete the proof, we use [47, eq. (5)]

$$\operatorname{erfc}(z) \leq e^{-z^2} \text{ for } z \geq 0. \quad (185)$$

- 2) The trigonometric identity $\cos^2 t + \sin^2 t = 1$ and the bound $\sin t \leq t$ (for $t \geq 0$) imply that

$$\cos^2 t \geq 1 - t^2. \quad (186)$$

Since the exponential function is monotone, we have

$$e^{-a \sin^2 t} \geq e^{-at^2}. \quad (187)$$

By combining the two inequalities, we obtain

$$\cos^2 t e^{-a \sin^2 t} \geq (1 - t^2)e^{-at^2}. \quad (188)$$

■

REFERENCES

- [1] A. Demir, A. Mehrotra, and J. Roychowdhury, "Phase noise in oscillators: a unifying theory and numerical methods for characterization," *IEEE Trans. on Circ. and Sys. I: Fund. Theory and App.*, vol. 47, no. 5, pp. 655–674, 2000.
- [2] E. Casini, R. D. Gaudenzi, and A. Ginesi, "DVB-S2 modem algorithms design and performance over typical satellite channels," *Int. J. on Sat. Comm. and Net.*, vol. 22, no. 3, pp. 281–318, 2004.
- [3] G. Durisi, A. Tarable, and T. Koch, "On the multiplexing gain of MIMO microwave backhaul links affected by phase noise," in *IEEE Int. Conf. on Comm. (ICC)*, Budapest, Hungary, Jun. 2013.
- [4] R. Tkach and A. Chraplyvy, "Phase noise and linewidth in an InGaAsP DFB laser," *J. Lightwave Tech.*, vol. 4, no. 11, pp. 1711–1716, 1986.
- [5] A. Viterbi, "Phase-locked loop dynamics in the presence of noise by Fokker-Planck techniques," *Proc. IEEE*, vol. 51, no. 12, pp. 1737–1753, 1963.
- [6] M. Katz and S. Shamai, "On the capacity-achieving distribution of the discrete-time noncoherent and partially coherent AWGN channels," *IEEE Trans. Inf. Theory*, vol. 50, no. 10, pp. 2257–2270, Oct. 2004.
- [7] P. Hou, B. Belzer, and T. Fischer, "On the capacity of the partially coherent additive white Gaussian noise channel," in *IEEE Int. Sym. Inf. Theory (ISIT)*, Yokohama, Japan, Jul. 2003, pp. 372–372.
- [8] A. Lapidoth, "Capacity bounds via duality: A phase noise example," *Asian-European Workshop on Information Theory*, pp. 58–61, Jun. 2002.
- [9] J. Dauwels and H.-A. Loeliger, "Computation of information rates by particle methods," *IEEE Trans. Inf. Theory*, vol. 54, no. 1, pp. 406–409, Jan. 2008.
- [10] L. Barletta, M. Magarini, and A. Spalvieri, "Estimate of information rates of discrete-time first-order Markov phase noise channels," *IEEE Photonics Tech. Lett.*, vol. 23, no. 21, pp. 1582–1584, Nov. 2011.
- [11] D. Arnold, H.-A. Loeliger, P. Vontobel, A. Kavcic, and W. Zeng, "Simulation-based computation of information rates for channels with memory," *IEEE Trans. Inf. Theory*, vol. 52, no. 8, pp. 3498–3508, Aug. 2006.
- [12] L. Barletta, M. Magarini, and A. Spalvieri, "The information rate transferred through the discrete-time Wiener's phase noise channel," *J. Lightwave Tech.*, vol. 30, no. 10, pp. 1480–1486, May 2012.
- [13] —, "A new lower bound below the information rate of Wiener phase noise channel based on Kalman carrier recovery," *Optics Express*, vol. 20, no. 23, pp. 25 471–25 477, Nov. 2012.
- [14] A. Barbieri and G. Colavolpe, "On the information rate and repeat-accumulate code design for phase noise channels," *IEEE Trans. Commun.*, vol. 59, no. 12, pp. 3223–3228, Dec. 2011.
- [15] G. Durisi, A. Tarable, C. Camarda, and G. Montorsi, "On the capacity of MIMO Wiener phase-noise channels," in *Inf. Theory and App. Workshop (ITA)*, Feb. 2013, pp. 1–7.
- [16] G. Durisi, A. Tarable, C. Camarda, R. Devassy, and G. Montorsi, "Capacity Bounds for MIMO Microwave Backhaul Links Affected by Phase Noise," *IEEE Trans. Commun.*, vol. 62, no. 3, pp. 920–929, Mar. 2014.
- [17] B. Goebel, R. Essiambre, G. Kramer, P. Winzer, and N. Hanik, "Calculation of mutual information for partially coherent Gaussian channels with applications to fiber optics," *IEEE Trans. Inf. Theory*, vol. 57, no. 9, pp. 5720–5736, Sep. 2011.
- [18] L. Barletta and G. Kramer, "On continuous-time white phase noise channels," in *IEEE Int. Sym. Inf. Theory (ISIT)*, Honolulu, HI, Jun. 2014.
- [19] —, "Signal-to-noise ratio penalties for continuous-time phase noise channels," *Int. Conf. on Cog. Rad. Oriented Wireless Net. (CROWN-COM)*, Jun. 2014.
- [20] G. Foschini and G. Vannucci, "Characterizing filtered light waves corrupted by phase noise," *IEEE Trans. Inf. Theory*, vol. 34, no. 6, pp. 1437–1448, Nov. 1988.
- [21] G. Foschini, L. Greenstein, and G. Vannucci, "Noncoherent detection of coherent lightwave signals corrupted by phase noise," *IEEE Trans. Commun.*, vol. 36, no. 3, pp. 306–314, Mar. 1988.
- [22] G. Foschini, G. Vannucci, and L. Greenstein, "Envelope statistics for filtered optical signals corrupted by phase noise," *IEEE Trans. Commun.*, vol. 37, no. 12, pp. 1293–1302, Dec. 1989.
- [23] A. Lapidoth and S. Moser, "Capacity bounds via duality with applications to multiple-antenna systems on flat-fading channels," *IEEE Trans. Inf. Theory*, vol. 49, no. 10, pp. 2426–2467, Oct. 2003.
- [24] H. Ghozlan and G. Kramer, "On Wiener phase noise channels at high signal-to-noise ratio," in *IEEE Int. Sym. Inf. Theory (ISIT)*, Istanbul, Turkey, Jul. 2013, pp. 2279–2283.
- [25] —, "Multi-sample receivers increase information rates for wiener phase noise channels," in *IEEE Global Telecom. Conf. (GLOBECOM)*, Atlanta, GA, Dec. 2013, pp. 1919–1924.
- [26] —, "Phase modulation in Wiener phase noise channels with oversampling at high SNR," in *IEEE Int. Sym. Inf. Theory (ISIT)*, Honolulu, HI, Jun. 2014.
- [27] R. Pighi and R. Raheli, "Information rates of oversampled detectors for transition-noise-limited digital storage systems," in *IEEE Int. Sym. Inf. Theory (ISIT)*, Nice, France, Jun. 2007, pp. 2536–2540.
- [28] E. Gilbert, "Increased information rate by oversampling," *IEEE Trans. Inf. Theory*, vol. 39, no. 6, pp. 1973–1976, 1993.
- [29] T. Koch and A. Lapidoth, "Increased capacity per unit-cost by oversampling," *IEEE Convention of Electrical and Electronics Engineers in Israel (IEEEI)*, pp. 684–688, Nov. 2010.
- [30] M. Dörpinghaus, G. Koliander, G. Durisi, E. Riegler, and H. Meyr, "Oversampling Increases the Pre-Log of Noncoherent Rayleigh Fading Channels," *IEEE Trans. Inf. Theory*, vol. 60, no. 9, pp. 5673–5681, Sep. 2014.
- [31] R. Martalo, A. Gervasi, C. Tripodi, and R. Raheli, "Information rate analysis of the oversampled phase-noise channel," in *Proc. Intern. Symp. Wireless Commun. Sys. (ISWCS)*, Aug. 2015.
- [32] J. Scarlett, *Reliable communication under mismatched decoding*. Ph.D. Thesis, University of Cambridge, 2014.
- [33] L. Barletta and G. Kramer, "Lower bound on the capacity of continuous-time Wiener phase noise channels," in *IEEE Int. Sym. Inf. Theory (ISIT)*, Hong Kong, Jun. 2015.
- [34] M. Martalò, C. Tripodi, and R. Raheli, "On the information rate of phase noise-limited communications," in *Inf. Theory and App. Workshop (ITA)*, 2013.
- [35] Y. Dallal and S. Shamai, "An upper bound on the error probability of quadratic-detection in noisy phase channels," *IEEE Trans. Commun.*, vol. 39, no. 11, pp. 1635–1650, Nov. 1991.
- [36] —, "Performance bounds for noncoherent detection under Brownian phase noise," *IEEE Trans. Inf. Theory*, vol. 38, no. 2, pp. 362–379, Mar. 1992.
- [37] Y. Dallal, G. Jacobsen, and S. Shamai, "Analytical upper bounds for noisy phase optical communication invoking Gaussian quadratic functionals," *IEEE Photonics Tech. Lett.*, vol. 5, no. 7, pp. 855–858, Jul. 1993.
- [38] L. Barletta and G. Kramer, "Upper bound on the capacity of discrete-time Wiener phase noise channels," in *IEEE Inf. Theory Workshop (ITW)*, Jerusalem, Israel, Apr. 2015.
- [39] M. Martalò, C. Tripodi, and R. Raheli, "Simple upper bound on the information rate of the phase noise channel," *Electron. Lett.*, vol. 52, no. 7, pp. 517–519, Apr. 2016.
- [40] M. Azizoglu, *Phase Noise in Coherent Optical Communications*. Boston, MA, USA: Ph.D. Thesis, Massachusetts Institute of Technology, 1991.
- [41] S. Moser, "Capacity results of an optical intensity channel with input-dependent Gaussian noise," *IEEE Trans. Inf. Theory*, vol. 58, no. 1, pp. 207–223, Jan. 2012.
- [42] K. V. Mardia and P. E. Jupp, *Directional Statistics*. John Wiley and Sons Ltd., 2000.
- [43] H. Ghozlan and G. Kramer, "Interference focusing for mitigating cross-phase modulation in a simplified optical fiber model," in *IEEE Int. Sym. Inf. Theory (ISIT)*, Austin, TX, Jun. 2010, pp. 2033–2037.
- [44] Y. Dallal and S. Shamai, "Power moment derivation for noisy phase lightwave systems," *IEEE Trans. Inf. Theory*, vol. 40, no. 6, pp. 2099–2103, Nov. 1994.
- [45] J. Aldis and A. Burr, "The channel capacity of discrete time phase modulation in AWGN," *IEEE Trans. Inf. Theory*, vol. 39, no. 1, pp. 184–185, Jan. 1993.

- [46] I. Gradshtein and I. Ryzhik, *Table of integrals, series and products*. Academic Press, 2007.
- [47] M. Chiani and D. Dardari, "Improved exponential bounds and approximation for the Q-function with application to average error probability computation," in *IEEE Global Telecom. Conf. (GLOBECOM)*, vol. 2, Taipei, Taiwan, Nov. 2002, pp. 1399 –1402.